

---

Electronic Thesis and Dissertation Repository

---

8-5-2021 9:00 AM

## Expression of pannexin1 in brain metastases derived from lung cancer

Rober Abdo, *The University of Western Ontario*

Supervisor: Penuela Silvia, *The University of Western Ontario*

Co-Supervisor: Qi Zhang, *The University of Western Ontario*

A thesis submitted in partial fulfillment of the requirements for the Master of Science degree in Anatomy and Cell Biology

© Rober Abdo 2021

Follow this and additional works at: <https://ir.lib.uwo.ca/etd>

---

### Recommended Citation

Abdo, Rober, "Expression of pannexin1 in brain metastases derived from lung cancer" (2021). *Electronic Thesis and Dissertation Repository*. 8028.

<https://ir.lib.uwo.ca/etd/8028>

This Dissertation/Thesis is brought to you for free and open access by Scholarship@Western. It has been accepted for inclusion in Electronic Thesis and Dissertation Repository by an authorized administrator of Scholarship@Western. For more information, please contact [wlsadmin@uwo.ca](mailto:wlsadmin@uwo.ca).

## Abstract

Brain metastases (BMs) are the leading cause of cancer-related deaths, comprise the majority of central nervous system malignancies, and widely originate from non-small lung carcinomas (NSCLC). Immunotherapy, particularly checkpoint inhibitors, has emerged as the standard of care for most patients with advanced lung cancer. Pannexin1 (PANX1) is a transmembrane glycoprotein that forms large-pore channels and has been reported to promote tumorigenesis in metastatic cancers. The roles of PANX1 in lung cancer-associated brain metastases and tumor-infiltrating lymphocytes have not been identified. Forty-two patient-matched formalin-fixed paraffin-embedded tissue samples from lung carcinomas and subsequent brain metastases were constructed into two master-tissue microarrays (TMAs). PANX1, PD-L1, and tumor-infiltrating immune cells (CD3+, CD4+, CD8+, and CD68+) were assessed using immunohistochemistry and digital image analysis (QuPath software). The expression of PANX1 was significantly higher in brain metastases than paired primary lung carcinoma. Strikingly, the level of PANX1 in lung carcinoma cells in the brain correlated negatively with the infiltration density of blood-derived macrophages. Our findings highlight the role of PANX1 in the progression of metastatic NSCLC, and the potential therapeutic approach of targeting PANX1 enhances the efficacy of immune checkpoint inhibitors in brain metastasis.

**Keywords:** Pannexins, Pannexin1, Lung cancer, Non-small cell lung carcinoma, Brain metastases, Tumor-immune infiltration, Tumor-associated macrophages.

## Summary for Lay Audience

Cancer from other parts of the body can spread to the brain. This is known as brain metastasis, the leading cause of cancer-related deaths. Brain metastases comprise the majority of brain tumors and widely originate from lung cancer. Immunotherapy approaches have emerged as the standard of care for most patients with advanced lung cancer. However, the difference in brain metastasis progress and response to immunotherapies among lung cancer patients requires robustly predictive- cellular parameters. Pannexin1 (PANX1) is a cellular protein that forms large-pore channels and has been reported to promote aggressiveness in multiple cancers. The roles of PANX1 in brain metastasis and immune responses have not been identified. Therefore, we studied 42 patient specimens obtained from lung cancers and their migratory cells in the brain and eventually conducted biological staining to assess the profiles of PANX1 and immune cells within cancer compartments. We found that PANX1 was higher in brain metastases compared to primary lung cancer. Immune cells known as macrophages that digest harmful structures and/or present them to T cells (cancer cells' killers) were less in brain metastasis cases with high levels of PANX1. These findings indicate the role of PANX1 in cancer progression and the immunological profile of advanced lung cancer.

## **Co-Authorship statement**

The work was carried out and written by the author, under the supervision of Dr. Silvia Penuela and Dr. Qi Zhang, who designed the project, procured funding, supervised its performance, and assisted with data analysis and editing of the manuscript.

Danielle Jonhston provided technical assistance with immunofluorescence staining and confocal imaging. Linda Jackson-Boeters assisted with immunohistochemistry staining for PANX1 and sectioning some TMA blocks. In addition, the technicians in the University Hospital of London conducted immunohistochemistry staining for TTF1, CK7, and CK20.

## Acknowledgments

Gratefulness overflows me due to the profluent welcoming value of Canada for immigrant refugees. I would also thank North Park Community Church in London for restructuring and solidifying my ambitions, particularly Ron Burdock and Donna Ballantine.

For my supervisors: Dr. Silvia Penuela and Dr. Qi Zhang, thank you for your support, mentorship, belief in my potential, and providing an embracive and friendly work environment. I would also like to thank my advisory committee: Dr. Trevor Shepherd, Dr. Shawn Whitehead, and Dr. Alison Allan, for their mentorship and assistance in developing this project. I would like to thank Dr. Silvia Penuela's laboratory members: Rafael, Brent, Brooke, Garth, Rober, Samar, and the undergrad students in the lab, for your insights, feedback, and creating an enjoyable workplace. For Dr. Qi Zhang's laboratory members: Haiyin Zheng, Carolyn Twible, Soumiya Suresh, Peter Liu, Abdulaziz Bholat, and Chelsey Zhao, thank you for your inputs and assistance. For Danielle Johnston, Linda Jackson, and the pathologists in the University Hospital of London, thank you for assisting me in conducting experiments.

I would additionally thank my wife, Misao, for your support and courage. For our newborn daughter, Humi, and kids, Ippei and Niko, thank you for creating a joyful environment that nourishes my perseverance. Finally, for my mother, Lousin, thank you very much for your love and sacrifice.

I dedicate my thesis to the memory of my father.

## Table of Contents

Abstract.....	ii
Summary for Lay Audience .....	iii
Co-Authorship statement.....	iv
Acknowledgments .....	v
Table of Contents.....	vi
Section 1: Introduction.....	1
1.1 Non-small cell lung carcinoma (NSCLC).....	2
1.2 Brain metastases.....	3
1.3 Genomic profiles of brain metastases derived from NSCLC .....	8
1.4 The immune microenvironment in brain metastases.....	9
1.5 Immune profiles in brain metastases derived from NSCLC .....	12
1.6 Treatment of brain metastases from NSCLC .....	13
1.7 Pannexins.....	14
1.8 Pannexin1 .....	17
1.9 Pannexin1 in the respiratory system.....	20
1.10 Pannexin1 and immune cell recruitment .....	20
1.11 Pannexin1 in cancer and metastasis .....	21
1.12 Rationale .....	23
1.13 Hypothesis.....	24
1.14 Aims .....	24
2.1 Patient Cohort .....	26
2.2 Tissue Microarray (TMA) .....	28
2.3 Immunohistochemistry (IHC) .....	30
2.4 QuPath Software .....	30
2.5 Immunofluorescence .....	33
2.6 Statistical Analysis.....	33
Section 3: Results .....	35
3.1 Metastatic cells in the brain retained the immuno-histochemical profile and strongly correlated with their primary tumors. ....	36

3.2 Protein levels of PANX1 were significantly higher in brain metastases compared to corresponding primary lung tumors.....	38
3.3 Brain metastases exhibited higher levels of $\beta$ -catenin compared to NSCLC	41
3.4 There was no statistical correlation between PANX1 levels of NSCLC and metastatic time interval.....	43
3.5 PANX1 distributed predominately in the cytoplasm of carcinoma cells in primary NSCLC and corresponding brain metastasis. ....	45
3.6 High levels of PANX1 were associated with less infiltration of blood-derived macrophages in brain metastases. ....	47
Graphical Summary.....	54
Section 4: Discussion .....	55
Limitation of the study and future directions .....	61
References.....	63
Section 5: Supplementary Figures.....	76

## List of Figures

Figure 1. Cancer cell metastatic dissemination to the brain.....	7
Figure 2. Schematic representation of human PANX1 protein.....	19
Figure 3. Schematic Structure of TMAs.....	29
Figure 4. Illustration of QuPath software annotation .....	32
Figure 5. Brain metastases preserve the immunohistochemical profile of NSCLC .....	37
Figure 6. PANX1 expression is higher in brain metastases compared to matched- NSCLC. ....	40
Figure 7. $\beta$ -catenin expression is higher in brain metastases compared to NSCLC.. ....	42
Figure 8. There is no significant correlation between the PANX1 level of NSCLC and metastatic time intervals.....	44
Figure 9. PANX1 is distributed predominantly in the cytoplasm in NSCLC and brain metastases.. ....	46
Figure 10. The densities of CD3+, CD8+, and CD68+ cells are higher in NSCLC compared to BM.. ....	49
Figure 11. There is no correlation between PD-L1 and PANX1 in NSCLC or BM. ....	51
Figure 12. PANX1 of lung carcinoma cells is associated with less infiltration of blood-derived macrophages in BM.....	53



Figure S.1. Expression of PANX1 had a positive correlation between primary NSCLC and matched metastatic lymph nodes .....	77
Figure S.2. Additional thresholds of PANX1 in primary NSCLC determined by quartile and tertile .....	78
Figure S.3. Expression of PANX1 in breast tumors or melanoma and matched-brain metastases .....	79
Figure S.4. Figure S.4. Brain metastasis cores are negative for the microglia marker, TMEM119. ....	80
Figure S.5. Infiltrated CD68+ cells in brain metastasis regions are macrophages derived from blood .....	81
Figure S.6. There is no correlation between the infiltration level of CD8+ or CD68+ cells and the metastatic time interval .....	82

## List of Abbreviations

<b>β-catenin</b>	Beta-catenin
<b>CRC</b>	colorectal cancer
<b>IHC</b>	Immunohistochemistry
<b>TKIs</b>	tyrosine kinase inhibitors
<b>ADC</b>	adenocarcinoma
<b>aRMS</b>	alveolar rhabdomyosarcoma
<b>BBB</b>	blood-brain barrier
<b>BMDMs</b>	bone marrow-derived macrophages
<b>CK20</b>	Cytokeratin 20
<b>CK7</b>	Cytokeratin 7
<b>CSF</b>	blood-cerebrospinal fluid
<b>CT</b>	carboxyl Termini
<b>CXs</b>	Connexins
<b>EGFR</b>	Epidermal growth factor receptor
<b>EL</b>	extracellular loops
<b>EMT</b>	Epithelial-mesenchymal transition
<b>ER</b>	endoplasmic reticulum
<b>eRMS</b>	embryonal rhabdomyosarcoma
<b>Gly</b>	glycosylation
<b>HCC</b>	hepatocellular carcinoma
<b>HER2</b>	human epidermal growth factor receptor 2
<b>ICIs</b>	immune checkpoint inhibitors
<b>kDa</b>	Kilo dalton
<b>LD</b>	leukodystrophy disease
<b>NAT</b>	normal adjacent tissues to brain metastases
<b>NSCLC</b>	Non-small cell lung carcinoma
<b>NT</b>	Amino termini
<b>OS</b>	Overall survival

<b>PANX1</b>	Pannexin1
<b>PANX2</b>	Pannexin2
<b>PANX3</b>	Pannexin3
<b>PANXs</b>	Pannexins
<b>PD-1</b>	Programmed death-1
<b>PD-L1</b>	Programmed death-ligand1
<b>RCC</b>	renal cell carcinoma
<b>SCC</b>	squamous cell carcinoma
<b>SRS</b>	stereotactic radiosurgery
<b>TAMs</b>	Tumor-associated macrophages
<b>TILs</b>	tumor-infiltrating lymphocytes
<b>TIME</b>	tumor immune microenvironment
<b>TM</b>	transmembranes
<b>TMA</b>	Tissue Microarray
<b>TTF1</b>	thyroid transcription factor 1
<b>WBRT</b>	whole-brain radiation therapy

# Section 1: Introduction

## 1.1 Non-small cell lung carcinoma (NSCLC)

Lung cancer leads to the largest number of cancer-related deaths worldwide<sup>1</sup>.

It is classified into two main histological groups: small cell lung carcinoma (SCLC, 15% of all lung cancers) and non-SCLC (NSCLC, 85% of all lung cancers). NSCLCs are generally subcategorized into adenocarcinoma (ADC, ~50%), squamous cell carcinoma (SCC, ~40%), and large cell carcinoma (~10%)<sup>2</sup>. In general, ADCs arise in more distal airways, whereas SCCs arise in more proximal airways and are more associated with smoking and chronic inflammation than ADCs<sup>3,4</sup>. ADCs often have glandular histology and express persistent biomarkers with an origin in the distal lung, including thyroid transcription factor 1 (TTF1; also known as NKX2-1) and keratin 7 (KRT7)<sup>3,4</sup>. However, SCCs are characterized by squamous differentiation and distinguished from ADCs in the clinic by immunostaining for cytokeratin 5 and cytokeratin 6 and/or the transcription factors SRY-box 2 (SOX2) and p63<sup>3-5</sup>. Large cell carcinoma is diagnosed with exclusion if tumor cells do not have glandular or squamous morphology or express ADC or SCC biomarkers<sup>3</sup>. Epidermal growth factor receptor (EGFR) and K-RAS mutations are the most prevalent- identified drivers of NSCLC in East Asia, Caucasian cohort, and Vietnamese cohorts<sup>6</sup>. Advances in next-generation sequencing (NGS) and other genomic profiling platforms have allowed researchers to examine the latitude of genetic mutations within lung tumors. After identifying KRAS and BRAF mutations<sup>7,8</sup>, epidermal growth factor receptor (EGFR) mutations were discovered in patients with lung ADC and were associated with response to

EGFR inhibitors<sup>9-12</sup>. In a recent study<sup>13</sup>, 256-Chinese patients with NSCLC were enrolled. NGS-based genomic profiling of central lung cancer-related genes was performed on a formalin-fixed paraffin-embedded tumor sample and found higher frequencies of anaplastic lymphoma kinase (ALK) and BRAF alterations were associated with younger age. The frequency of mutations in EGFR was significantly higher in nonsmokers than in smokers<sup>13</sup>. It has been revealed that  $\beta$ -catenin is essential for the development of *EGFR*-mutated lung cancers<sup>14</sup>. Pharmacologic inhibition of  $\beta$ -catenin suppressed *EGFR*-mutated lung tumor growth, and genetic deletion of the  $\beta$ -catenin gene dramatically reduced lung tumor formation in mutated-*EGFR* transgenic mice<sup>14</sup>. Therefore,  $\beta$ -catenin is critical for lung carcinoma progression.

## 1.2 Brain metastases

An estimated 20% of cancer patients develop brain metastases (BMs)<sup>15</sup>; however, autopsy studies have suggested higher incidences (up to 40%) of intracranial metastases in patients with tumors<sup>16</sup>. While any tumor can metastasize to the brain, the three most prevalent primary tumors associated with brain metastases are lung (40–56% of patients), breast (5–20%), and melanoma (7–16%)<sup>17-19</sup>. Lung cancer is the most predominant to metastasize to the brain regardless of patient sex and is the most common brain metastasis in men, whereas breast cancer is the most commonly occurring brain metastasis in women<sup>15</sup>. The molecular phenotype of the primary tumor could influence the risk of developing brain metastases. For instance, women with

breast cancers characterized by human epidermal growth factor receptor 2 (ERBB2, also known as HER2) amplification or triple-negative hormone receptor status (that is, estrogen receptor (ER)-negative, progesterone receptor (PR)-negative and normal HER2 levels) have a higher risk of developing brain metastases than those with ER-positive and/or PR-positive breast cancer<sup>20</sup>. Likewise, ALK-rearranged NSCLC has a higher tendency to metastasize to the brain. Advanced primary cancer disease also influences the risk of progressing brain metastasis<sup>21</sup> and intensifies the likelihood of its emergence<sup>22</sup>; however, the time interval from initial cancer diagnosis to the development of brain metastases is highly influenced by the primary cancer type<sup>23</sup>. In a study, the time interval for patients with breast cancer to develop brain metastases was 44 months, whereas it was 11 months for lung cancer<sup>17</sup>. Other contributing factors to the development of brain metastases entail ethnicity, age, and geographic location. A study demonstrated that African Americans with lung cancer, melanoma, and breast cancer had a higher incidence of brain metastases than other ethnic groups with the same cancer types<sup>24</sup>. In contrast, renal cell carcinoma (RCC)-brain metastases in African Americans were lower than in white patients. The risk of brain metastases also differs with age regardless of the tumor phenotype<sup>24,25</sup>. For example, in one study, the risk of breast cancer brain metastases was highest in younger patients (20–39 years of age), but the risk of lung cancer brain metastases was highest in middle age (40–49 years of age); melanoma, RCC and colorectal

cancer (CRC) - brain metastases arose with the highest risk a decade later (50–59 years of age).

Brain metastases develop upon disseminating cells from a primary tumor through the blood to the brain microvasculature despite potential occurrence from established metastases. As illustrated in (Figure 1), tumor cells initially detach from the primary tumor, acquire stem cell-like properties, resulting in an epithelial-mesenchymal transition, and invade the surrounding tissues, venules, capillaries, and lymphatic system<sup>91</sup>. Tumor cell interactions with immune cells promote cell motility via clearance of extracellular matrix. In the circulation, tumor cells undergo adhesive-circulatory arrest within the vasculature and extravasate, either as single cells or emboli. The abundance of capillary networks in the brain and high blood flow causes a high exposure to circulating tumor cells. A circulatory arrest is enhanced by slowed movement at branch points in capillaries (~3–7  $\mu\text{m}$  in diameter), as well as the larger size of tumor cells (up to 20  $\mu\text{m}$ ) compared with deformable red blood cells (7  $\mu\text{m}$ )<sup>28,29</sup>. Tumor cells permeate the disruptive brain functional barriers, blood-brain barrier (BBB)<sup>30</sup>, and blood-cerebrospinal fluid (CSF) barrier<sup>31</sup>. Brain metastases tend to occur at the junction between grey and white matter and watershed areas between vascular territories, where it is proposed that circulating tumor cells benefit from longer relative mean transit times of blood flow, enabling more time for the cells to overcome the blood-brain barrier and exit from the vasculature<sup>15</sup>. After arresting and extravasating, most tumor cells die rather than form metastases, whereas others can lie dormant at metastatic sites for extended periods<sup>32</sup>. Tumor cell



interplays with the brain microenvironment lead to the outgrowth of tumor cells and cancer-specific signaling pathways<sup>19</sup>. Metastases are envired by a neuroinflammatory response<sup>33</sup>, including activated astrocytes, microglia, and immune cells, which will be discussed in the following section.

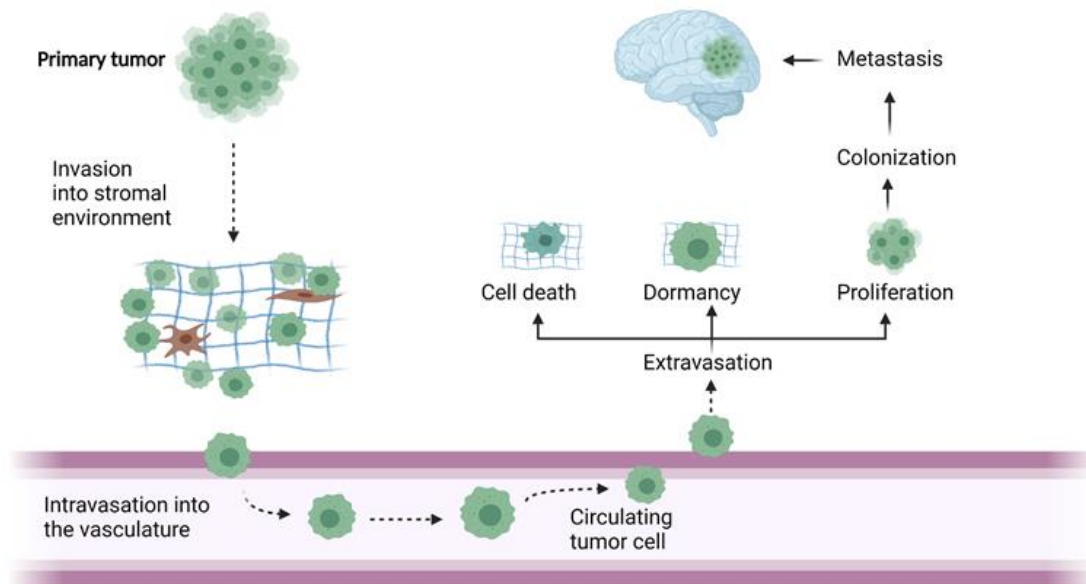


**Figure 1. Cancer cell metastatic dissemination to the brain.** Brain metastases develop after the hematogenous spread of cells from a primary lung tumor to the brain microvasculature, with subsequent tumor growth enhanced by microenvironmental niche–tumor interactions. Initially, tumor cells escape primary bulk tumors and invade the surrounding tissues. Once in the circulation, circulating tumor cells establish the process of metastatic extravasation from the vasculature. After extravasating, most tumor cells die rather than form metastases, whereas others can lie dormant at metastatic sites for extended periods. The figure was drawn on BioRender and modified from *Achrol et al.*<sup>15</sup>. The green color indicates lung carcinoma cells, whereas the brown refers to stromal cells.

### 1.3 Genomic profiles of brain metastases derived from NSCLC

Brain metastases are diagnosed in more than a quarter of patients with stage IV NSCLC<sup>34</sup>. Approximately 10–21% of lung tumors are initially diagnosed with brain metastasis, and 50–60% will develop into brain metastases during the course of the disease<sup>35</sup>. While a role of PD-1, LKB1, KRAS, and EGFR mutations and ALK rearrangements has been associated with the progression of lung cancer<sup>36,37</sup>, their presumptive pathogenesis of brain metastases is still debatable<sup>37,38</sup>. Detailed genomic profiling of primary NSCLC and matched brain metastases was performed with next-generation sequencing targeting 416 cancer-relevant genes on 61 patients who had surgical resection of primary NSCLC and brain metastases<sup>39</sup>. In this study, mutations of major drivers, including EGFR, KRAS, TP53, and ALK, were highly universal between primary NSCLC and matched brain metastases (>80%), while discordance suggested the exclusive oncogenic mechanisms of NSCLC brain metastases. Altered cell cycle regulators and PI3K pathway were more enriched in brain metastases, and activated PI3K signaling correlates with shorter survival<sup>39</sup>. In the study of Villalva et al.<sup>40</sup>, molecular alterations of KRAS, EGFR, and ALK were present in 39%, 3.9%, and 7.7% of brain metastases, respectively. The concordance percentage of the EGFR mutations in paired primary NSCLCs and brain metastases ranges between 36% and 100%<sup>41–44</sup>. Therefore, testing EGFR mutations in the primary site of NSCLC may not be informative for using EGFR tyrosine kinase inhibitors (TKIs) to treat brain metastases. However, a significant bulk of NSCLCs has no

molecular alterations; therefore, there is a need to investigate other potential targetable biomarkers.

#### **1.4 The immune microenvironment in brain metastases**

Intercommunication between tumor cells and cellular members of the microenvironment sustains normal tissue homeostasis and supports tumor growth. This intercellular communication is operated by a dynamic network of cytokines, chemokines, growth factors, and enzymes remodeling the extracellular matrix, leading to profound changes in properties of the surrounding tissue<sup>45,46</sup>.

The brain was previously considered an immunologically privileged organ because the healthy brain has almost no lymphocytes<sup>46</sup>. However, the central nervous system is a specialized immune site under a regulatory network linking native brain cells and lymphocytes<sup>47</sup>. In established brain metastases, the inflammatory tumor microenvironment comprises the innate immune system, microglia, blood-derived myeloid cells/macrophages, and the adaptive immune system, essentially represented by T cells<sup>48</sup>. Microglia are the critical cells of the innate immune system in the brain. Physiologically, microglia are motile and constantly move through the brain parenchyma<sup>49</sup>. Therefore, microglia cells reside heterogeneously within the healthy brain<sup>50</sup>. The differences in microglia distribution were observed early during the process of extravasation in brain metastasis preclinical models, indicating that microglia may be involved in extravasation and survival in the perivascular niche<sup>33</sup>. Microglia functions in brain metastasis encompass antigen presentation, cytotoxicity via expression of nitric oxide (NO) and superoxide, and phagocytosis<sup>49</sup>. A crucial function of microglial

cells in brain metastasis is T-cell activation upon expression of the HLA ABC/major histocompatibility antigen class I. Therefore, microglial activation is essential for inducing a specific immune response, including T and B cells<sup>49</sup>.

PD-L1 expression, the ligand of the inhibitory T-cell co-receptor PD1, is expressed on microglia cells and can suppress T-cells<sup>51</sup>. Microglia with phagocytic activities is a member of the tumor-association macrophages (TAMs) population within brain metastasis, including blood-derived macrophages<sup>33</sup>. Two functional phenotypes of TAMs have been proposed. The M1 TAMs are defined by tumor-suppressive functions like inhibition of cell proliferation<sup>52</sup>. The M2 TAMs have tumor-promoting functions, including suppressing the adaptive immune response and promoting tumor cell migration, invasion, and intravasation into the vascular system, angiogenesis, and persistent growth<sup>52</sup>. There was previously no specific biomarker to differentiate resident microglia and bone marrow-derived macrophages BMDMs<sup>53</sup>. CD49D and TMEM 119 have recently been identified as differential markers between BMDMs and microglia<sup>53,54</sup>. These studies also proposed that most TAMs in the brain metastases were derived from peripheral monocytes and not from resident microglia.

Lymphocytes generally are not present in the brain parenchyma and migrate into the CNS under pathological condition<sup>55</sup>. Several subtypes of tumor-infiltrating lymphocytes (TILs) can be found in the brain metastasis ' inflammatory microenvironment and vary in physiology and prognostic significance<sup>56</sup>. CD3+ TILs represent the overall population of effector T cells. CD8+ TILs represent cytotoxic T-cell, whereas CD4+ TILs reflect helper T cells. FOXP3+/CD25+/CD4+

TILs are called regulator T cells and have immunosuppressive function<sup>57</sup>. They inhibit the function of CD8+ cytotoxic T-cell and contribute to an immune suppressive microenvironment. Characteristics of the primary tumor can influence the T cell response in brain metastases. A denser TIL infiltration was observed in brain metastases derived from melanoma and RCC compared with those derived from breast cancer and non-small lung carcinoma<sup>58</sup>. Brain metastases' patients with dense infiltration of effector CD3+ or cytotoxic CD8+ had an improved survival prognosis from diagnosis compared with patients with absent or fewer infiltration of TILs<sup>57</sup>. The immune response is physiologically counterbalanced by inhibitory pathways, which prevent uncontrolled immune response; these inhibitory pathways are immune checkpoints that maintain the immune homeostasis<sup>59,60</sup>. In cancer, tumor cells typically express immune checkpoints to halt the antitumor immune responses against them as an adaptive escape mechanism<sup>61</sup>. Among the discovered immune checkpoints, the interaction between programmed death 1 receptor (PD-1) on T- cells and its ligand programmed death-ligand 1/2 (PD-L1/2) on tumor cells or TILs as well as the interplay between cytotoxic T-lymphocyte-associated protein 4 (CTLA-4) on T-cells and its ligand B7-1 (CD80) or B7-2 (CD86) on tumor cells or TILs. These immune checkpoint pathways have been identified as critical immunosuppressive mechanisms in cancer<sup>62,63</sup> and, therefore, candidate targets. Nevertheless, the education of immune cell types in the brain TME depends on tumor origin.

## 1.5 Immune profiles in brain metastases derived from NSCLC

Characterization of the immune profiles is beneficial to provide a better understanding basis for the precise treatment of brain metastasis. In mixed cohorts (N = 252) of brain metastasis patients, the immune infiltrates distribution was analyzed<sup>58</sup>. The authors described a highly heterogeneous distribution of the immune infiltrates across brain metastases with three major patterns observed: perivascular stromal infiltration (typically observed in NSCLC and other carcinomas), peritumoral infiltration (lymphocytes surrounding brain metastases), and homogeneously diffuse infiltration (usually observed in melanoma). There was no association between TILs, and overall survival (OS). Other studies have demonstrated that TILs can infiltrate the stroma and peritumoral parenchyma of brain metastases<sup>64</sup>. However, a high density of CD3+ or CD8+ cells was positively correlated with OS<sup>56</sup>. Spatial diversity of immune infiltrates in matched primary tumors and corresponding brain metastases was observed in patients with NSCLC. Primary lung tumors had more positive TILs and PD-L1 expression than brain tumor metastases<sup>65</sup>. In another study containing a cohort of 20 paired NSCLC primary tumor and brain metastases samples, T-cell receptor sequencing showed a significant reduction of T-cell clones in brain metastases compared with paired primary lung tumors despite the higher mutation burden in brain metastases<sup>66</sup>. Furthermore, lower T-cell densities were documented in brain metastases than primary lung tumors after sequencing T-cell receptor beta (TCR $\beta$ ) in a cohort of 78 samples from NSCLC primary tumors and paired brain metastases. Nonetheless, the authors found a high frequency of shared T-cell

clones between matched samples and proposed that the tumor microenvironment of brain metastasis was more immunosuppressed than the primary tumor. Accordingly, studies have investigated the T cell function and distribution in advanced NSCLC lesions to identify a novel scheme to enhance anti-tumor T cell immunity. However, insights into the role of the diversified-myeloid compartment at NSCLC sites are lacking.

### **1.6 Treatment of brain metastases from NSCLC**

The majority of medical therapies for brain metastases include systemic chemotherapies alongside whole-brain radiation therapy (WBRT) or stereotactic radiosurgery (SRS), as well as molecular and immunotherapeutic approaches aimed at shrinking tumors or inhibiting their growth<sup>15</sup>. The identification of driver mutations in NSCLC has been translational in the management of brain metastases. The most recent National Comprehensive Cancer Network NSCLC guidelines (2019 version 4) recommend that tumor tissue needs to be tested for EGFR, KRAS, HER2, ALK, ROS1, MET, BRAF, RET, and NTRK mutations<sup>67</sup>. EGFR and ALK-targeted therapies are well established in oncogenic-driven NSCLC and shown to have good CNS penetration, achieving intracranial response rates between 40% and 80%<sup>68</sup>. Although a large number of patients have oncogenic-driven NSCLC, a substantial proportion of patients do not have such molecular alterations. The advancement of immune checkpoint inhibitors (ICIs) has opened a new avenue of cancer treatment. Immunotherapy with PD-1 or PD-L1 inhibitors is a generally accepted treatment option for patients with advanced lung cancer, whether as a single treatment or in combination with



chemotherapy<sup>69,70</sup>. In the first-line KEYNOTE-189 trial<sup>69</sup> and the second-line OAK trial<sup>71</sup>, patients with immunotherapy-treated brain metastasis showed a more prolonged overall survival (OS) than chemotherapy-treated. A recent phase 2 trial reported that pembrolizumab had effectiveness in brain metastasis from NSCLC with PD-L1 expression at least 1%<sup>72</sup>. However, the efficacy of anti-PD-1/PD-L1 treatments is improved in only a subset of brain metastasis patients. There are still ongoing clinical trials assessing predictive biomarkers for the effectiveness of ICIs in advanced NSCLCs. Nonetheless, recent discoveries have shed light on the role of TME in tumor progression and therapy. ATP encompasses a major component of TME<sup>73</sup>, communicates with immune cells, and regulates their functions. A significant membrane channel that conducts ATP is pannexins, which will be discussed in the following section.

## **1.7 Pannexins**

Pannexins (PANXs) are a glycoprotein family of three members (PANX1, PANX2 & PANX3) that form channels for the passage of ions and other metabolites involved in cell signalling<sup>74-76</sup>. They were discovered because of their limited sequence homology to the invertebrate innexin gap junction proteins, and it was initially considered that they could form gap junctions as vertebrate gap junction proteins, connexins (CXs)<sup>74</sup>. Nonetheless, it soon became clear that the gap junction function of PANXs is not their primary function, and there is a significant sequence disparity between PANXs and CXs<sup>77</sup>. PANXs exhibit a similar topology to CXs with four  $\alpha$ -helical transmembrane (TM) domains, two extracellular loops

(EL), and one intracellular loop (IL), with their amino (NT) and carboxyl (CT) termini exposed to the cytoplasm<sup>74,78</sup>.

The NT region is the most preserved domain, but the highest sequence variance is found in the CT domain<sup>79</sup>. PANX1 and PANX3 are more analogous to each other compared to PANX2<sup>80</sup>. Originally it was reported that six subunits of PANXs oligomerize to form a channel, and these oligomers are named 'pannexons' that refer to single-membrane channels<sup>81</sup>. In contrast, the term 'connexons' for connexins refers to 'hemichannels' (i.e., a structure constituting half of a cell-cell channel)<sup>82</sup>. Recently, the structure of PANX1 has been revealed, and the channel is now known to be formed by seven subunits<sup>83</sup>. PANX1 and PANX3 genes are both located on chromosome 11, have (41%) sequence similarity, and their proteins contain 426 (~48kDa) and 392 (~45kDa) amino acids, respectively<sup>78</sup>. PANX2 gene is located on chromosome 22 and encodes the largest protein among pannexin family members, containing 677 amino acids (~73kDa)<sup>80</sup>.

Pannexins are co-translationally embedded into the endoplasmic reticulum (ER)<sup>84</sup> and subsequently modified by N-linked-glycosylation that mediates cellular localization of pannexins<sup>80,85</sup>. The glycosylation sites for PANX1 (N254) and PANX3 (N71) were found to be in the second extracellular loop and the first extracellular loop, respectively, whereas the site for PANX2 glycosylation is on the first extracellular loop (N86)<sup>85</sup>. PANXs could be present as un-glycosylated proteins (Gly0) or as high mannose species (Gly1) that mainly localize intracellularly<sup>81,85</sup>. PANX1 and PANX3 are eventually transported to the Golgi

apparatus and acquire more complex glycosylation (Gly2). Pannexins are primarily localized at the cell membrane in this form<sup>85</sup>. Early on in this pathway, pannexin monomers oligomerize and form non-selective channels that permit the flux of molecules up to 1kDa in size, including ions and ATP<sup>75</sup>.

Despite the variance of sequences between pannexins and connexins, pannexins show a matching structure to connexin hemichannels, and therefore, they were initially proposed as a new gap junction family<sup>79,86</sup>. Nonetheless, PANX1 and PANX3 can stay at the cell surface for more than 21 hours, but connexins have a short half-life (1-5 hours)<sup>85,87,88</sup>. Additionally, pannexins distribute throughout the cell membrane while connexins show particular assembling at cell-to-cell contacts<sup>89</sup>. Gap junction formation by PANXs could be prevented by glycosylation of the pannexin proteins<sup>80,81,90</sup>.

Pannexins have been identified in various cell types and tissues<sup>75</sup>. While PANX1 is widely expressed, PANX2 and PANX3 expression is more selective<sup>75</sup>. PANX3 has been reported in the skin, bone, and cartilage, including keratinocyte, chondrocyte, and osteoblast. Panx3 has additionally been found in the lung, liver, kidney, spleen, and thymus of 3-week-old three mice<sup>91,92</sup>. PANX2 was initially thought to be expressed only in the central nervous system; however, it has recently been identified in the skin, skeletal muscle, and the spleen<sup>93</sup>. The expression of PANX1 will be discussed in the following section.

## 1.8 Pannexin1

It was long thought that PANX1 monomer proteins oligomerize into hexameric channels<sup>75,94,95</sup> (Figure 2). However, recent research groups independently revealed similar cryo-electron microscopy structures of the PANX1 channel that appeared to be assembled in a homomeric heptamer<sup>83,96–98</sup>. This oligomerization occurs intracellularly, mainly in the ER<sup>99</sup>, and then PANX1 can be trafficked to the cell surface, where they have been characterized as conduits for ATP release<sup>100,101</sup>. Under normal physiological conditions, Panx1 channels are considered to be closed<sup>92</sup>. PANX1 is reportedly stimulated by several physiological mechanisms<sup>95,102</sup>, including signaling pathways mediated by membrane receptors<sup>103,104</sup>, elevated extracellular potassium<sup>105</sup> or intracellular calcium levels<sup>104</sup>, proteolytic cleavage by caspases<sup>100</sup>, hypoxemia<sup>106</sup> and membrane stretch, and voltage<sup>107</sup>. PANX1 channels can be closed by negative feedback from extracellular ATP<sup>108</sup> and by PANX1 channel blockers<sup>109</sup>. Studies have proposed that the PANX1 channel may be regulated by the carboxy-terminal end, which could reversibly close the pore<sup>110</sup>. However, cleavage of the carboxy-terminal end by caspase 3 or 7 can open and activate the channel<sup>100</sup>. PANX1 is the most characterized member of the three pannexins, presumably because of its widespread expression in mammalian tissues<sup>75,111</sup>. Studies have identified PANX1 expression in the heart, liver, testis, small intestine, ovary, placenta, thymus, lung, pancreas, spleen, colon, and blood<sup>86</sup>. PANX1 expression has also been found in different mouse brain structures, including the cerebral cortex, hippocampus, cerebellum, and brain stem<sup>112</sup>. The presence of the PANX1

protein in the skin, kidney, and ear cartilage has also been documented, and the cardiac ventricular wall in 3-week-old C57BL/6 mice<sup>80</sup>.

The first physiological role attributed to PANX1 was a passage pathway for ATP, allowing the outflow of ATP to function as a signal to cells via activation of purinergic receptors<sup>101</sup>. Crucial evidence for ATP release mediated by PANX1 channels includes the localization of PANX1 expression corresponding to ATP release at the apical membrane of polarized epithelial cells such as in the airways or renal tubules<sup>113,114</sup>. Depletion of Panx1 channels additionally diminishes ATP release<sup>108,110,115</sup>. PANX1 mutations and chemical modification of the protein affect ATP release<sup>116,117</sup>. The ATP release-role of PANX1 has been shown to affect Ca<sup>2+</sup> waves, regulating the release of nitric oxide (NO) in the smooth muscle of blood vessels and resulting in vasodilation when erythrocytes respond to shear stress or hypoxia<sup>104</sup>. PANX1-associated ATP from leukemic cells undergoing apoptosis can act as a “find me” signal and attract macrophages and monocytes<sup>100</sup>. PANX1 channels can efflux inflammation-associated cytokines upon an interaction between HIV1 and CD4+ cells<sup>103,118</sup>. Increased levels of extracellular K<sup>+</sup> released in the brain activate PANX1 channels and release ATP that causes neuronal hyperactivity in seizures of juvenile mice<sup>119</sup>.

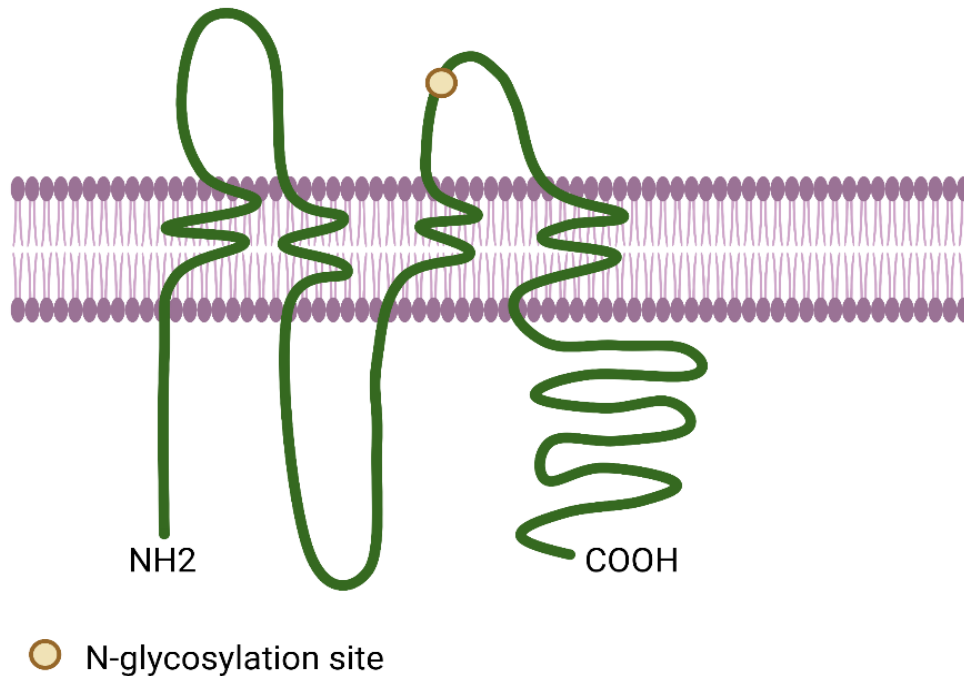


**Figure 2. Schematic representation of human PANX1 protein.** PANX1 was proposed as a tetra-spanning membrane protein with two extracellular loops and amino and carboxyl termini exposed to the cytoplasmic side. N-linked glycosylation site of PANX1 at N254 (yellow circle). The figure was generated using BioRender.

## **1.9 Pannexin1 in the respiratory system**

ATP is a paracrine regulator of airway epithelial cell functions. Quantitative-PCR showed PANX1 expression in normal human airway epithelial cells during re-differentiation at the air-liquid interface (ALI); immunohistochemistry confirmed PANX1 expression at the apical pole of airway epithelia and Goblet cells<sup>113</sup>.

Genetic or pharmacological suppression of PANX1 expression in differentiated airway epithelial cells hindered ATP release upon hypotonic stress by 60%<sup>113</sup>.

Additionally, PANX1 plays a role in the inflammatory component of asthma, where inhibition of PANX1 in a murine model of asthma reduced the infiltration of eosinophils in the peribronchial region<sup>120</sup>. Endothelial PANX1 has been shown to play a vital role in regulating lung vascular inflammation and edema in response to ischemia/reperfusion injury<sup>121</sup>.

## **1.10 Pannexin1 and immune cell recruitment**

Recruitment of inflammatory cells to the injury site is driven by plenty of signals that influence cell-cell interactions between vascular endothelial cells and circulating leukocytes. In acute inflammation induced by tumor necrosis factor-alpha (TNF $\alpha$ ), PANX1 channels have been found to assist in the adhesion and extravasation of leukocytes through the vascular wall<sup>122</sup>.

PANX1 channels have been reported to play a role in the chemotaxis response of neutrophils. Indeed, the activation of the chemoattractant receptors on the surface of neutrophils controls PANX1-induced ATP release, which subsequently stimulates P2Y2 receptors<sup>123</sup>. PANX1 channels play a role in generating

multinucleated macrophages<sup>124</sup>, the activation of T-cells<sup>125</sup>, and the migration of leukocytes during inflammation<sup>123</sup>. In a cytokine-induced colitis model of human colonic mucosal strips, the mucosal strips had less severe structural damage in the PANX1 channel-blocker incubated group than the cytokines-only group<sup>126</sup>. PANX1 channels have been linked to immune cell recruitment in leukemic cells, releasing ATP as find-me signals for monocytes and macrophages, which may regulate the crosstalk with other immune cells<sup>100</sup>. However, PANX1 enhances ATP-mediated T cell death *in vitro*<sup>127</sup>. Although PANX1 is implicated in the process of inflammation and cell death, no study has looked at the role they play in tumor-infiltrating lymphocytes *in vivo*. Nonetheless, a recently published study has found that PANX2 mRNA expression in low-grade glioma had a significant negative correlation with several immune cells, especially with macrophage, dendritic cells, and CD4+ T cells<sup>128</sup>.

### **1.11 Pannexin1 in cancer and metastasis**

Upregulation or amplification of PANX1 was documented in human biopsies from most tumor types according to the analysis of cross-cancer alterations in the 89 cancer studies included on the cBioPortal.org for Cancer Genomics<sup>129</sup>. Panx1 expression is listed in 17 out of 20 tumor types (high in colorectal, lung, urothelial, and stomach cancers) (Human Protein Atlas<sup>130</sup>). Elevated expression or an enhanced function of PANX1 have primarily been linked to the onset or progression of cancer<sup>111</sup>. PANX1 expression has been reported at all stages of human melanoma<sup>131</sup>; inhibition or deletion of PANX1 channels reduces the growth, migration, and invasiveness of the melanoma cells<sup>131</sup> as well as the



number of liver metastasis from mouse melanomas in a chicken embryo model<sup>132</sup>. A gain-of-function mutation in PANX1 channels enhances the metastatic capability of breast cancer cells, particularly to the lung in a mouse model<sup>107</sup>. At the same time, a pharmacological blockade or genetic deletion of PANX1 everts epithelial-mesenchymal transition (EMT) in human breast cancer-cell lines<sup>133</sup>.

Moreover, overexpression of PANX1 increased invasion and migration of testicular cancer cells, whereas genetic or pharmacological suppression of the channel decreased tumorigenesis of the cells<sup>134</sup>. In hepatocellular carcinoma (HCC), PANX1 promoted the invasion and metastasis of HCC cells *in vitro* and *in vivo* and was an independent prognostic factor for HCC patients<sup>135</sup>. Additional illustrations include the human glioma cell line U87-MG that significantly declined proliferation after PANX1 siRNA treatment<sup>136</sup>. Similarly, higher expression of PANX1 is found in human leukemic lymphocytes compared to normal T cells<sup>137</sup> and in aggressive multiple myeloma cell lines<sup>138</sup>. Therefore, PANX1 plays a role in the progression of multiple tumors.

Although most reports in the literature demonstrated an increased level of PANX1 in cancer cells, there are also important exceptions. A study documented that although PANX1 mRNA was expressed in primary astrocytes, the C6 rat glioma cell line did not express it, and overexpression of PANX1 in C6 glioma cells resulted in tumor suppression<sup>139</sup>. The same authors of the study reported that four human glioma cell lines (U87, U251, SF188, and SF539) were positive for PANX1 at the transcript level, indicating some differences in PANX1

expression among species in gliomas<sup>139</sup>. Furthermore, PANX1 levels are significantly reduced in gallbladder adenocarcinoma compared to normal gallbladder epithelium and correlated to the proliferative activity of the cells<sup>140</sup>. Recently, a study has shown that PANX1 expression is down-regulated in cell lines of alveolar rhabdomyosarcoma (aRMS) and embryonal rhabdomyosarcoma (eRMS)<sup>141</sup>. These cases constitute the few notable exceptions to the general idea that PANX1 tends to be upregulated in tumors compared to normal tissues.

## 1.12 Rationale

The variance in brain metastasis progression and tumor-infiltrating immune profile among metastatic lung carcinoma patients requires robust- predictive biomarkers. The role of PANX1 in the progression and immune landscape of lung cancer-derived brain metastases has not been explored yet.

The criterion of clinical cancer treatment has deviated towards using immune checkpoint inhibitor (ICI) treatments. The ICIs have shown promising clinical effects in NSCLC<sup>142</sup>. However, only a subset of patients shows responsiveness to the treatment. The predictive and prognostic biomarkers for ICIs efficacy have considered the expression levels of immune checkpoint genes PD-1, PD-L1, CTLA4, and mutational burden in cancer samples<sup>143,144</sup>. The heterogeneity of the tumor microenvironment around tumor cells was not investigated<sup>144</sup>. TME significantly contributes to cancer development and malignancy<sup>145</sup>, and the tumor immune microenvironment (TIME) plays a significant role in tumor immune surveillance and immunological evasion<sup>146,147</sup>. In the TME, ATP significantly

impacts tumor progression and metastasis<sup>148</sup>; among the channels that conduct ATP across the plasma membrane are channels formed by PANX1<sup>100</sup>. Therefore, investigating the role of PANX1 in the crosstalk between lung carcinoma cells and immune cells is vital. There is no published work on the relationship between PANX1 and immune cells within a tumor, nor the correlation of PANX1 expression in the primary lung- and metastatic brain tumors.

### **1.13 Hypothesis**

PANX1 expression is upregulated in brain metastases compared to corresponding primary lung carcinomas and is linked with a lower density of tumor-infiltrating immune cells.

### **1.14 Aims**

- 1) Assess protein levels of PANX1 in brain metastases and patient-matched primary lung carcinomas.
- 2) Investigate the density of T-cells and macrophages in brain metastases and corresponding primary lung carcinomas in human specimens.

## Section 2: Methods

## **2.1 Patient Cohort**

This study was approved by the Western University Health Science Research Ethic Board (HSREB 111911). Forty-two patient-matched formalin-fixed- paraffin-embedded tissue (FFPE) samples of lung carcinomas in the lung and subsequent metastases in the brain between 2005 and 2015 were provided by the London Health Sciences Centre. The cohort contains 42 FFPE NSCLCs, where the majority of the cases are adenocarcinoma phenotype. The clinical-histological characteristics of the patients are described in table 1.

<b>Table 1. Patient Characteristics (n=42)</b>		
<b>Variable</b>	<b>Category</b>	<b>Number</b>
Sex	Male	15
	Female	27
Age	Median (range)	63 (46-97)
Histology	Adenocarcinoma	38
	Squamous cell carcinoma	3
	Large cell carcinoma	1
Pathology Stage (TNM) at the time of diagnosis	I	1
	II	23
	III	14
	IV	4
Time interval to metastasize	Median (range)	14 (0-120) months

## **2.2 Tissue Microarray (TMA)**

After performing 4 $\mu$ m sections, slides were reviewed by local pathologists using hematoxylin and eosin-stained preparations<sup>149</sup> to select representative tumor areas. Each case was represented by three cores (0.6 mm<sup>2</sup> each) obtained from a primary lung carcinoma block followed by three cores constructed from matched-brain metastasis block and eventually arrayed in two recipients TMA-master-blocks as illustrated in figure 3. Finally, FFPE specimens of the non-tumor brain and placenta were used as controls. The histological diagram below describes the structure of our TMA<sup>150,151</sup>.

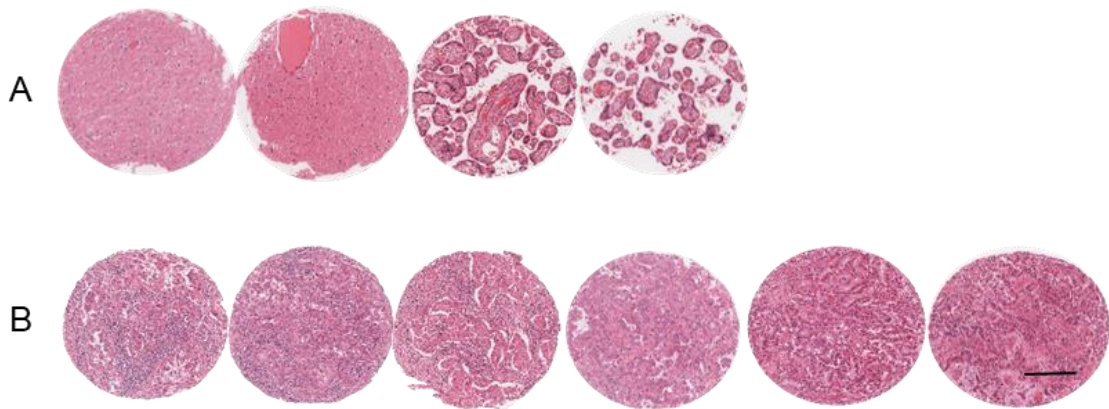


**Figure 3. Schematic Structure of TMAs.** The first row was obtained from FFPE human non-tumor brain tissues (A1 and A2) and placenta (A3 and A4) and used as a control and instructor. Each case was represented by three cores constructed from primary lung tumor block (cores B1, B2, and B.3) followed by three cores obtained from matched brain metastasis block (cores B4, B5, and B6). Scale bar= 200  $\mu$ m.



## 2.3 Immunohistochemistry (IHC)

IHC was performed on four  $\mu\text{m}$ -thick sections from TMA master blocks. Slides were then immediately transferred to fresh 100% xylene and processed through an ethanol hydration gradient (100, 90, 70, 50% ethanol solutions for 5 min each) before immersion in distilled water. After deparaffinization, immunohistochemistry was performed as previously described<sup>152</sup>. Briefly, sections were washed thrice in phosphate buffer saline (PBS), boiled in 10mM sodium citrate solution for antigen retrieval, blocked in PBS with 2.5% horse serum for 1 hour, washed thrice with PBS, and eventually incubated overnight at 4 °C with primary antibodies. Anti-PANX1 antibody (1:200; rabbit polyclonal)<sup>80</sup>, anti-CD3 (1:500, mouse monoclonal, DAKO), anti-CD4 (4B12, mouse monoclonal, DAKO), anti-CD8 (1:250; Mouse monoclonal, DAKO), anti-CD68 (1 : 200; mouse monoclonal, Dako) and anti-PD-L1 (1:200; mouse monoclonal, DAKO), TTF1 (1:50; monoclonal, DAKO), CK7 (1:50; monoclonal, DAKO), CK20 (1:50; monoclonal, DAKO), and TMEM119 (1:100; Abcam).

## 2.4 QuPath Software

TMAAs were digitized and quantified using an open software QuPath<sup>153</sup> (<https://qupath.github.io/>), a digital pathology software to quantify stained images. It can process whole slide images up to 40 G.B. and evaluate IHC staining. It averages a variation of staining intensity with the ability to detect total tissue areas or areas of interest. The H-score takes into account both staining intensity

and percentage of cells stained, giving a range of 0–300 using the following formula:  $1 \times (\% \text{ cells } +) + 2 \times (\% \text{ cells } ++) + 3 \times (\% \text{ cells } +++)$ . Overall scores were averaged from triplicate cores for each tissue type in each patient, and a minimum of 200 tumor cells was evaluated. Initially, H & E slides from TMAs were reviewed then the representative areas of the tumor were annotated manually based on tumor histomorphology and confirmed by immunohistochemistry using Pan-CK. Necrotic and hemorrhagic regions were excluded. H&E annotations were copied on IHC stained TMAs to quantify protein levels (Figure 4). Cores unsuitable for analysis, either with no tumor tissue or significant artifacts, were excluded. H-Scores were also averaged from triplicate cores. The TMA cores below illustrate how to select tumor cells and exclude other<sup>153–155</sup>. CD3, CD4, CD8, CD68, and PD-L1 analysis were classified as either positive or negative for the marker and quantified as a percentage of positive cell numbers relative to lung carcinoma cell numbers<sup>58</sup>.

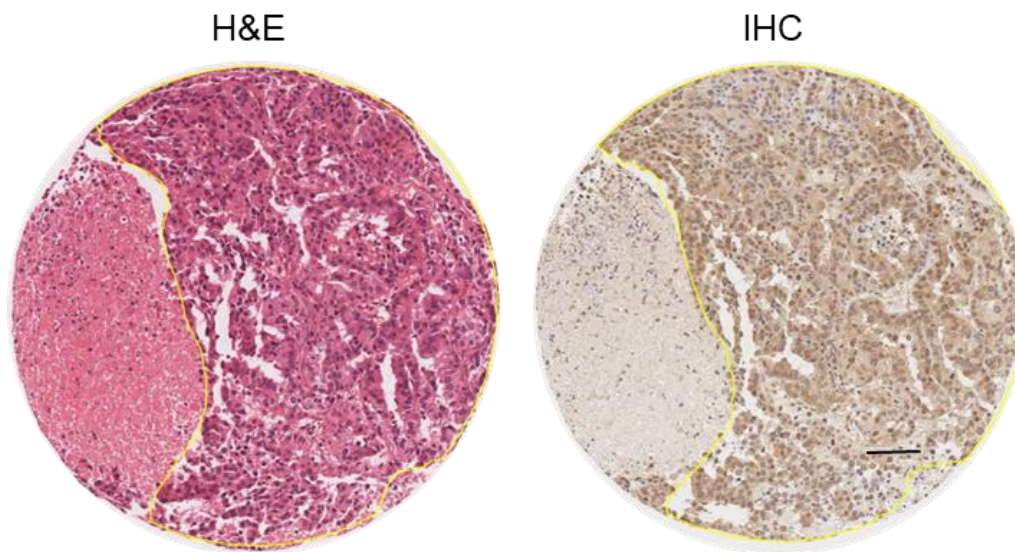


**Figure 4. Illustration of QuPath software annotation.** Manually, tumor cells in IHC-stained cores were annotated, and other cell types were excluded after histological analysis based on H&E-stained cores—Scale bar= 100  $\mu$ m.

## 2.5 Immunofluorescence

TMA blocks were sectioned into four  $\mu\text{m}$ -thick, deparaffinized, and immunolabeled with PANX1-CT primary antibody (stock 1  $\mu\text{g}/\mu\text{l}$ ) in a 1:100 dilution as described previously<sup>156</sup>. Briefly, slides were immersed with descending alcohol (100%, 95%, 70%, 50%) for rehydration, washed with PBS, and warmed in vector lab- antigen unmasking solution (H-3300), blocked with 3% B.S.A. and 0.1% Triton X-100 in PBS for an hour and then incubated with primary antibodies overnight at 4°C. Sections were washed three times with PBS and incubated with appropriate species-specific secondary antibodies conjugated with Alexa 488 or 647 for 60 minutes at room temperature and then counterstained with Hoechst to visualize nuclei. Sections were cover-slipped using a fluorogel mounting medium. Immunofluorescence images were obtained using a Zeiss LSM 800 Confocal Microscope with a Plan-Apochromat 63x/1.40 Oil DIC objective (Carl Zeiss). Peptide competition was conducted as described previously<sup>156</sup>.

## 2.6 Statistical Analysis

Statistical analyses were performed using GraphPad Prism (version 9.1.2). Comparison analysis is represented by a plot of symbols & lines with a graph family of a column as individual values. Correlation graphs were performed by computing Pearson correlation coefficients and displayed as a graph family XY. The correlation between metastatic time interval and a level of PANX1 in NSCLC was performed by a Kaplan-Meier Curve. The thresholds for PANX1 levels were

determined by tertiles and quartiles. p-values were calculated by parametric, paired-two-tailed Student's t-test for all graphs.

## **Section 3: Results**

### **3.1 Metastatic cells in the brain retained the immuno-histochemical profile and strongly correlated with their primary tumors.**

In the NSCLC-brain metastasis cohort, all metastatic cells in the brain specimens had the same immune profile as their matched-NSCLC specimens. They were positive for thyroid transcription factor 1 (TTF-1) and cytokeratin 7 (CK7) but negative for cytokeratin 20 (CK20) (Figure 5). The triple markers (TTF-1+, CK7+, CK20-) outline is widely used to diagnose primary NSCLC<sup>149</sup>. Figure 5 shows a positively strong correlation of TTF1 and CK7 between primary lung cases and their matched brain metastases.

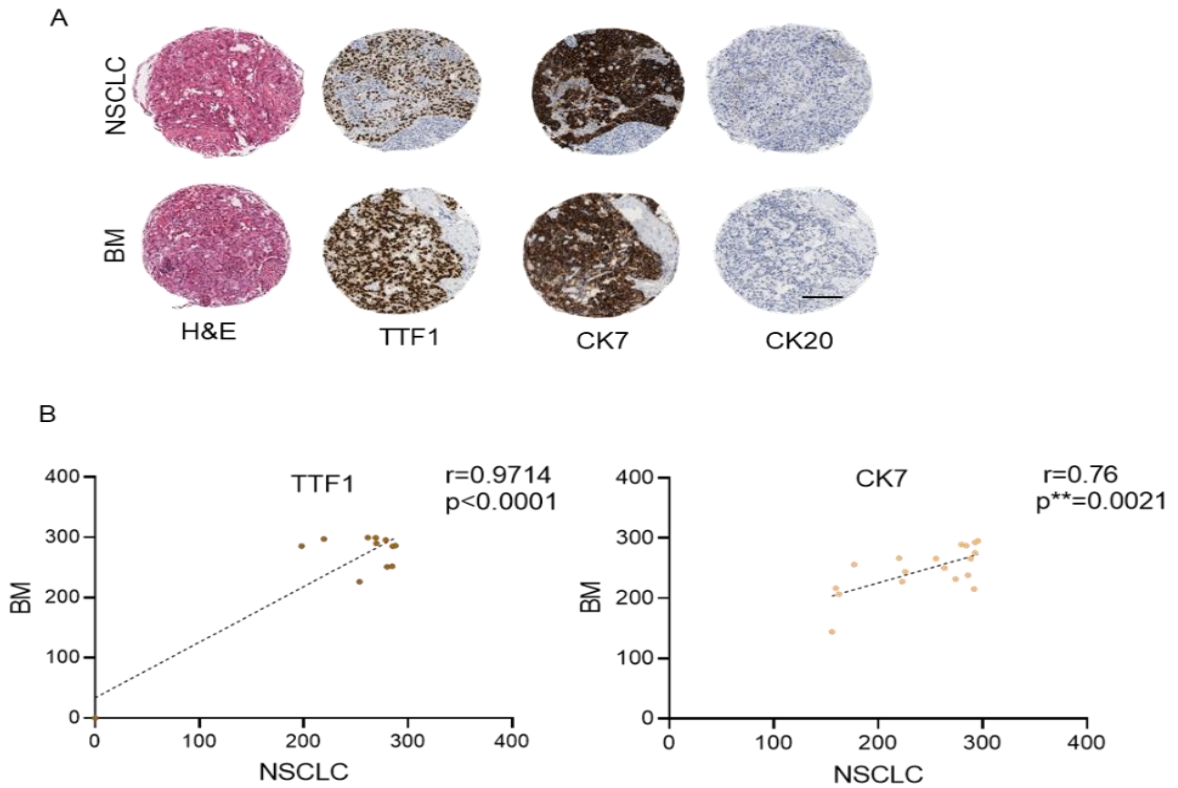


**Figure 5. Brain metastases preserve the immunohistochemical profile of NSCLC.** **A** representative image of IHC with antibodies raised against TTF1, CK7, and CK20 in primary NSCLC and matched-brain metastasis cores. Metastatic cells in the brain have the same immune-histology profile as in NSCLC tissue, indicating that the metastatic cells in the brain originated from lung carcinoma. Images are shown with a 200- $\mu$ m resolution. **B** Positive correlation of TTF /CK7 between NSCLC and brain metastases. Scatter Plot shows a positive correlation, where Pearson  $r>0.8+$  and  $p<0.0001$  for TTF-1,  $p=0.0024$  for CK 7, indicating a strong positive correlation.



### **3.2 Protein levels of PANX1 were significantly higher in brain metastases compared to corresponding primary lung tumors.**

Protein levels of PANX1 were assessed in the NSCLC-brain metastasis cohort (N=42 cases). Each patient was represented by three cores from an NSCLC sample and three cores from its matched sample of brain metastasis and constructed by TMA. TMA blocks were sectioned and stained independently with H&E and anti-PANX1 antibody<sup>131</sup>. H&E and PANX1 staining were visualized and then analyzed by QuPath; carcinoma cells of both samples were selected manually based on H&E morphology and confirmed by a pathologist. Next, the staining intensity of PANX1 in three cores of each representative sample was averaged, considering that (+) is weak staining, (++) is a medium staining, and (+++) is intense staining (Figure 6.A). The staining intensity was assessed using an H-score variable on QuPath software described above. Next, PANX1 levels (H-scores) in NSCLC and brain metastases were statistically compared. A protein level of PANX1 was significantly higher in brain metastases in comparison to matched-NSCLC (Figure 6.A). The correlation between PANX1 levels of primary NSCLC and PANX1 levels of brain metastasis was then assessed. Interestingly, PANX1 levels of NSCLC were strongly and positively correlated with PANX1 levels of brain metastases, where Pearson coefficient  $r$  was  $>0.6$  (Figure 6.B). This indicates that a level of PANX1 in an NSCLC may predict the level of PANX1 in a matched-brain metastasis case; an increase of a PANX1 level in lung carcinoma cells would lead to an increased level of PANX1 in metastasizing-lung carcinoma cells in the brain. Notably, the exact correlation

was found when assessing PANX1 levels of primary NSCLC and PANX1 levels of matched-metastatic lymph nodes in PANX1 (Supplementary section, Figure S1). Further, the expression of PANX1 was investigated in two smaller cohorts of brain metastasis patients with breast cancer and melanoma, and their analyses can be found in the supplementary figures section, figure S3.

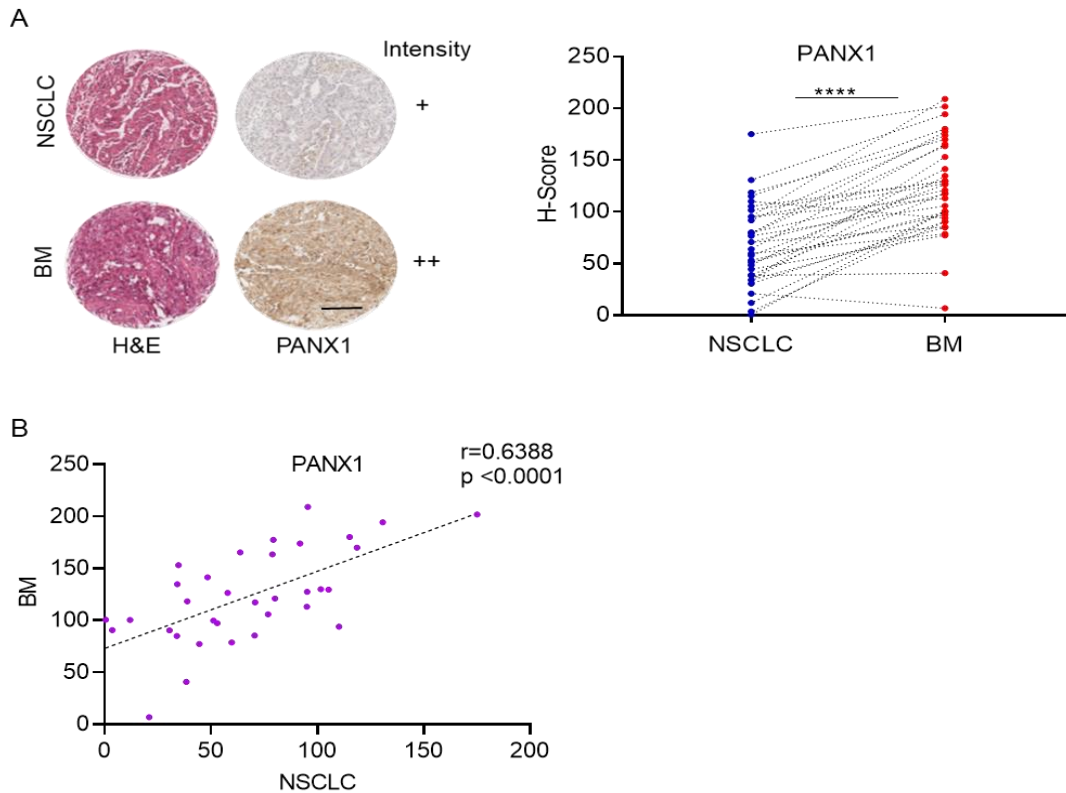


**Figure 6. PANX1 expression is higher in brain metastases compared to matched- NSCLC.** **A** representative image of I.H.C with an anti-PANX1 antibody on TMAs. The upper panel represents NSCLC cores, and the lower panel represents matched brain metastasis cores; representative areas of tumor were selected by analyzing the morphology of cores based on H&E- stained slides then traced carcinoma cells using QuPath software. Cores were categorized into 'intensity' groups (+, weak staining) and (++, medium staining). Images scanned at 20X objective magnification. Paired T-test of PANX1 levels between NSCLC and matched-brain metastases shows that PANX1 of brain metastases is significantly higher than PANX in NSCLC (\*\*\*\* $P < 0.0001$ ). The total number of cases was 42, but outliers were excluded ( $n=35$ ). Scale bar=100  $\mu$ m. **B** Scatter Plot shows a strong positive correlation between PANX1 levels in lung tumors and brain metastases (Pearson coefficient =0.63), and this correlation was statistically significant (\*\* $P > 0.0001$ ).

### **3.3 Brain metastases exhibited higher levels of $\beta$ -catenin compared to NSCLC**

Levels of  $\beta$ -catenin, a key member of the Wnt signaling pathway, were evaluated in brain metastases and NSCLC.  $\beta$ -catenin has been linked to enhancing metastasis in different tumors<sup>157–159</sup> and playing a role in lung tumorigenesis<sup>14</sup>. More importantly and recently, Sayedyahosseini et al. discovered a direct interaction between  $\beta$ -catenin and PANX1 in melanoma cells<sup>160</sup>. Additionally, it has been demonstrated that deletion of PANX1 pharmacologically or genetically decreased the levels of  $\beta$ -catenin and indicated a reverse of EMT in human breast cell lines<sup>133</sup>. Therefore,  $\beta$ -catenin levels were evaluated in NSCLC and brain metastases and tested a correlation between them. Levels of  $\beta$ -catenin were quantified in both samples using QuPath and then performed a paired t-test. The  $\beta$ -catenin level was significantly higher in brain metastases than in NSCLC (Figure 7.A). There was no significant correlation of  $\beta$ -catenin between NSCLC and brain metastases (Figure 7.B). Next, a correlation between  $\beta$ -catenin levels and PANX1 levels in NSCLC was tested. There was no statistically significant correlation (Figure 7.C).

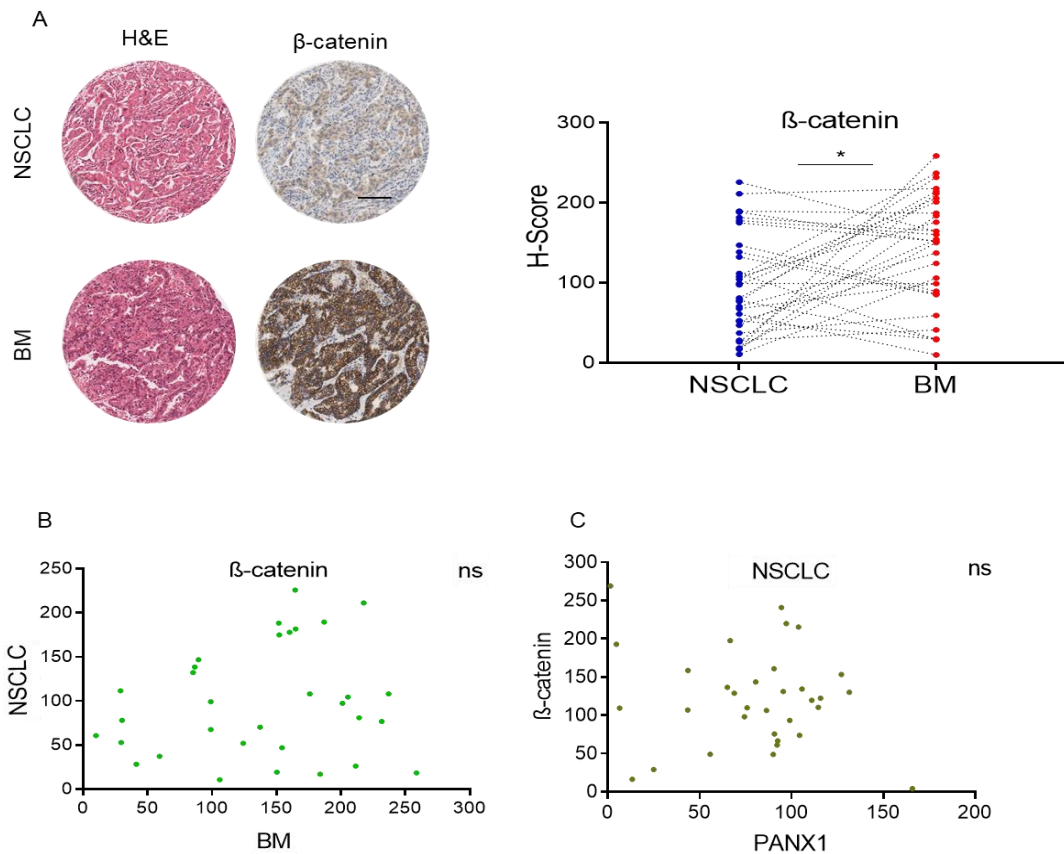


**Figure 7. β-catenin expression is higher in brain metastases compared to NSCLC.** **A** representative image of IHC with an antibody raised against β-catenin shows that the staining is more intense in BM. Paired T-test between β-catenin of NSCLC (blue dots) and beta-catenin of BM (red dots) shows a significant difference between the groups (\* $P=0.011$ ). Scale bar= 100 μm. **B** Scatter Plot of β-catenin levels in brain metastases and primary NSCLC shows no correlation, where Pearson variable ( $r=0.16$ ). **C** Scatter Plot between PANX1 and β-catenin levels in lung tumors shows no statistically significant correlation (Pearson  $r=-0.1355$ ).

### **3.4 There was no statistical correlation between PANX1 levels of NSCLC and metastatic time interval.**

The time interval of the NSCLC cases to metastasize to the brain ranges from (0-120) months. The Histogram (Figure 8.A) shows the distribution of the cases based on a time interval to metastasize to the brain, where most cases have a time interval of  $\geq 20$  months. A correlation between PANX1 levels of NSCLC and the time interval to metastasize to the brain was investigated. NSCLC cases were split into two groups, high PANX1 and low PANX1, determining the thresholds by a median, tertiles, and quartiles<sup>151</sup>, and applied the two groups on a survival curve (Figure 8.B); other thresholds are shown in figure S.2. There was no statistically significant correlation.

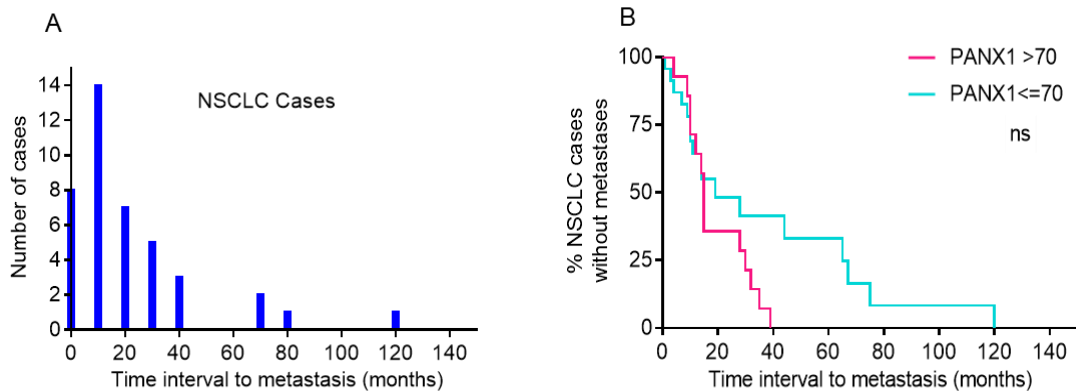


**Figure 8. There is no significant correlation between the PANX1 level of NSCLC and metastatic time intervals.** **A** Distribution of NSCLC cases (N=42) is displayed based on PANX1 (H-score) levels and a time needed to metastasize to the brain. **B** Survival curve between two groups of PANX1 level (high vs. low) in primary NSCLC and the time intervals to metastasize to the brain. The X-axis indicates the time intervals of primary NSCLC to metastasize, whereas the y-axis shows the percentage of NSCLC cases without brain metastases. Quartiles determined the thresholds of the PANX1 level (H-score).

### **3.5 PANX1 distributed predominately in the cytoplasm of carcinoma cells in primary NSCLC and corresponding brain metastasis.**

Next, the cellular localization of PANX1 was investigated to assess any differences between primary NSCLC and matched brain metastases. Therefore, immunofluorescent staining was performed on the TMA with an antibody raised against PANX1. PANX1 in the brain metastases and NSCLC specimens was located predominantly in intracellular compartments of carcinoma cells (Figure 9).



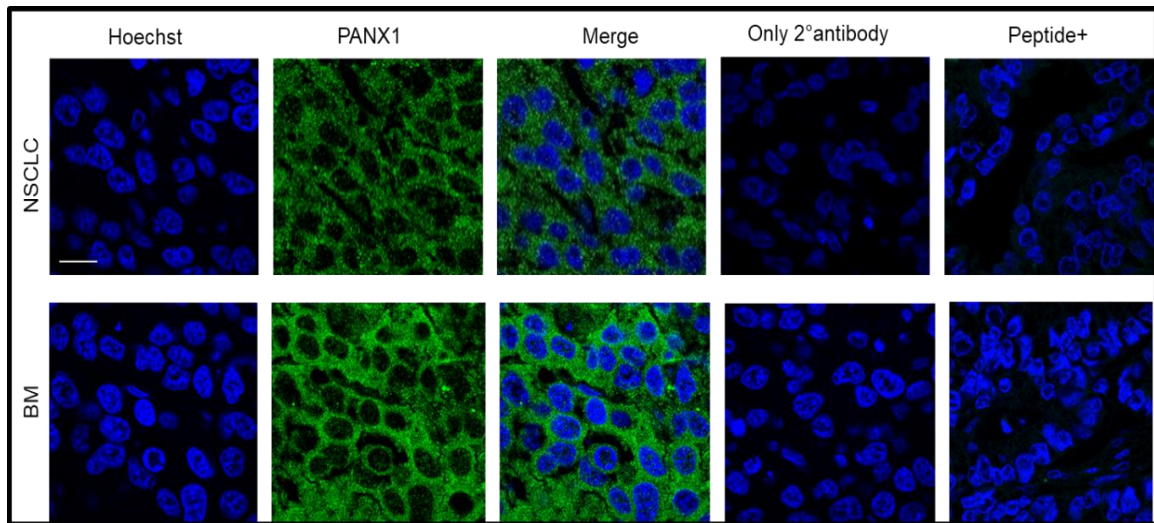


**Figure 9. PANX1 is distributed in the cytoplasm in NSCLC and brain metastases.** Representative images of IF (N=21) using an anti-PANX1 antibody in NSCLC (upper panel) and brain metastasis samples (lower panel). Hoechst staining is displayed in blue color, whereas PANX1 in green. The column (merge) has PANX1 staining and Hoechst staining. The columns (only secondary antibody and peptide+) show validation of the specificity of the anti-PANX1 antibody. PANX1 was mainly distributed intracellularly in lung carcinoma cells in the lung and brain. Scale bar=20 $\mu$ m.

### **3.6 High levels of PANX1 were associated with less infiltration of blood-derived macrophages in brain metastases.**

Next, the correlation between the level of PANX1 and the immune infiltration was assessed. Therefore, immunohistochemical staining was conducted independently on TMA using anti (CD3, CD4, CD8, CD68, and PD-L1) antibodies. First, the density of these immune markers was compared between NSCLC samples and their matched brain metastases using QuPath software, performing a percentage of positive cells for the immune marker relative to all lung carcinoma cells within each core and averaging the density in 3 cores of each case sample<sup>58</sup>. CD3+, CD8+, and CD68+ cells were more infiltrated in NSCLC (Figure 10.A) compared to their paired brain metastases. Next, the percentages of CD3+, CD8+, CD4+, and CD68+ cells infiltration to the total tumor were applied on a paired T-test and found the density of immune markers, CD3, CD8, and CD68, were significantly higher in NSCLC compared to their densities in brain metastases. In contrast, there was no statistical significance in CD4+ cell infiltration between NSCLC and brain metastases (Figure 10.B).

Because CD68 expression profiling does not precisely distinguish between peripherally derived macrophages and brain resident microglia, the expression of TMEM119 (a microglia marker)<sup>161</sup> was assessed using IHC on TMAs (Figure S.4). Cores of normal adjacent tissues to brain metastases (NAT) from the TMAs and external-brain tissues of leukodystrophy disease (LD) were used as positive controls for TMEM119. The analysis showed that most CD68+ immune cells in the brain metastases were negative for TMEM119 (Figure S.5); therefore, CD68+

cells represented blood-derived macrophages. Subsequently, an evaluation of the correlation between CD8+ or CD68+ cells infiltration in NSCLC and metastatic time intervals was performed. Lung tumor cases were split into two groups, high density of CD8+ or C68+ cells and low density of CD8+ or CD68+ cells, taking a median percentage as a threshold and applying the inputs on the survival curve. Neither the density of CD8+ cells nor the density of C68+ cells in NSCLC correlated with a time interval to metastasize to the brain (Figure S.6).

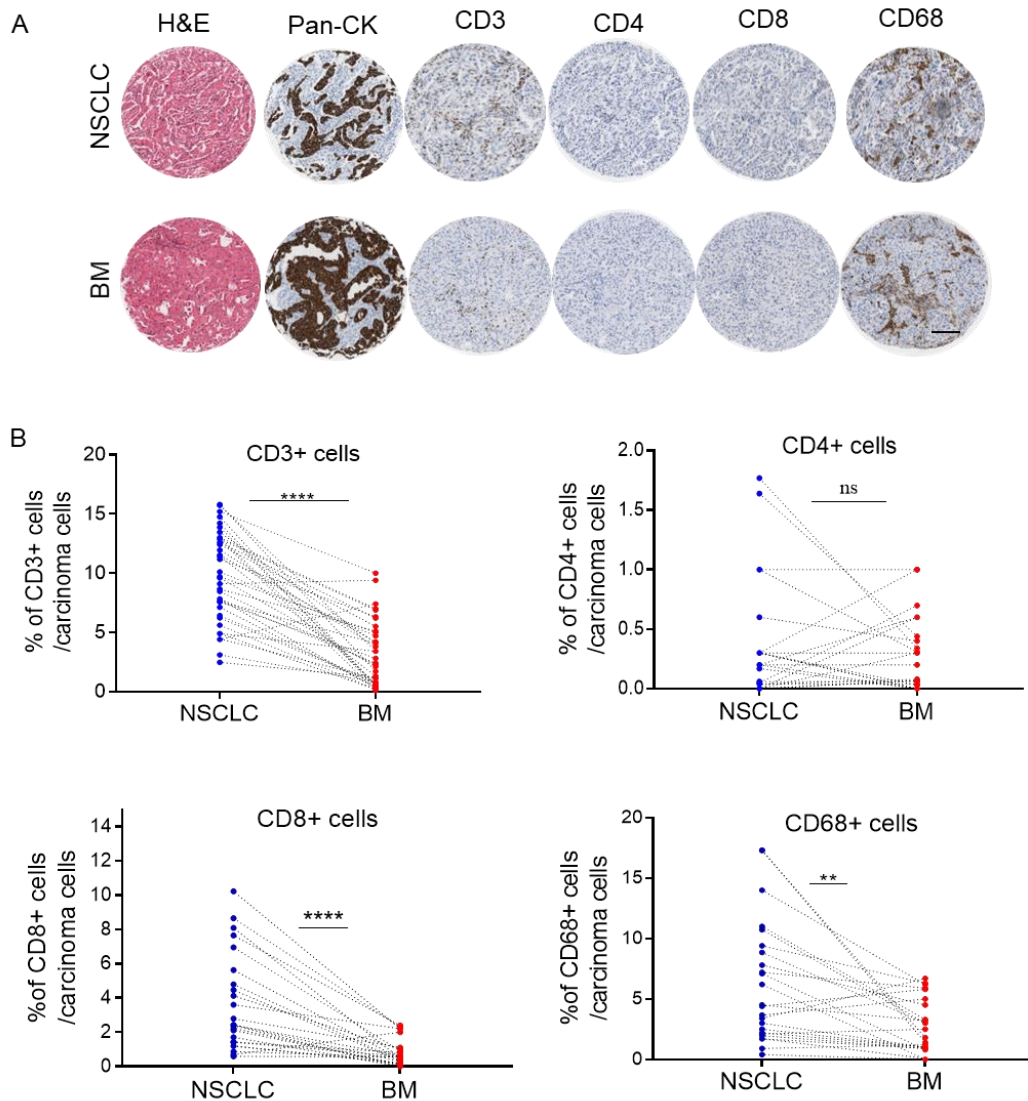


**Figure 10. The densities of CD3+, CD8+, and CD68+ cells are higher in NSCLC compared to BM.** **A** Representative image of H&E and IHC with antibodies raised against CD3, CD4, CD8, and CD68 on TMA slides. The density of these immune markers was assessed through QuPath software by performing a percentage of CD3, CD8, CD4, and CD68+ cells infiltration relative to all carcinoma cells within NSCLC and BM cores. Scale bar= 100  $\mu$ m. **B** Paired T-test was performed to compare the infiltration of these immune cells between NSCLC and BM. The test shows significantly higher infiltration of CD3, CD8, and CD68 in NSCLC compared to matched brain metastases, N=35, where outliers were excluded.

Additionally, due to the significance of PD-L1 expression level for the efficacy of ICIs in lung carcinoma<sup>143,162-165</sup>, PD-L1 levels of carcinoma cells were assessed by performing a percentage of PD-L1+ cells relative to all carcinoma cells within each core<sup>143</sup>. PD-L1 expression was higher in NSCLC compared to brain metastases (Figure 11.A). By performing a correlation plot between PANX1 levels and PD-L1 levels of carcinoma cells, there was no statistically significant correlation neither in NSCLC nor brain metastases (Figure 11.B).

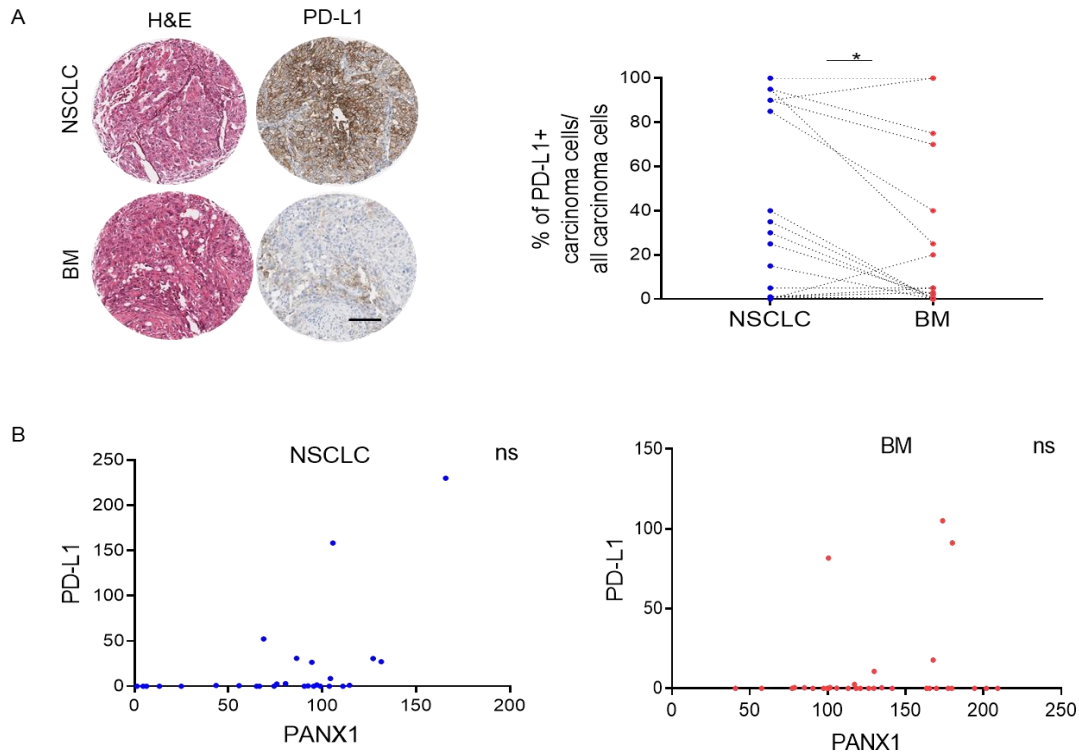


**Figure 11. There is no correlation between PD-L1 and PANX1 in NSCLC or BM.** **A** Representative image of NSCLC and BM cores was stained independently with H&E and PD-L1. PD-L1 expression was assessed using QuPath by the percentage of PD-L1+ carcinoma cells relative to total tumor cells within a core and then compared between NSCLC and BM using paired t-test. PD-L1 significantly expressed higher in NSCLC (\* $p=0.016$ ). Scale bar= 100  $\mu\text{m}$ . **B** Correlation plot was performed between PD-L1 of carcinoma cells and PANX1 of carcinoma cells in NSCLC and BM. There was no statistically significant correlation, where Pearson  $r=0.34$  and  $0.2$  respectively.

Next, a correlation was tested between PANX1 levels of carcinoma cells and CD3+, CD8+, or CD68+ cells infiltration. There was no correlation between PANX1 levels and the density of CD3+, CD8+ or CD68+ cells in NSCLC (Figure 12.A, B, &C). There was no correlation between PANX1 levels of carcinoma cells and the density of CD3+ or CD8+ cells in brain metastases (Figure 12.D &E). Interestingly, there was a negative correlation between PANX1 levels of carcinoma cells and the density of CD68+ cells in brain metastases. Pearson coefficient was (-0.405) (Figure 12.F), pinpointing that a higher level of PANX1 in metastatic lung carcinoma cells is associated with less infiltration of macrophages in the brain.

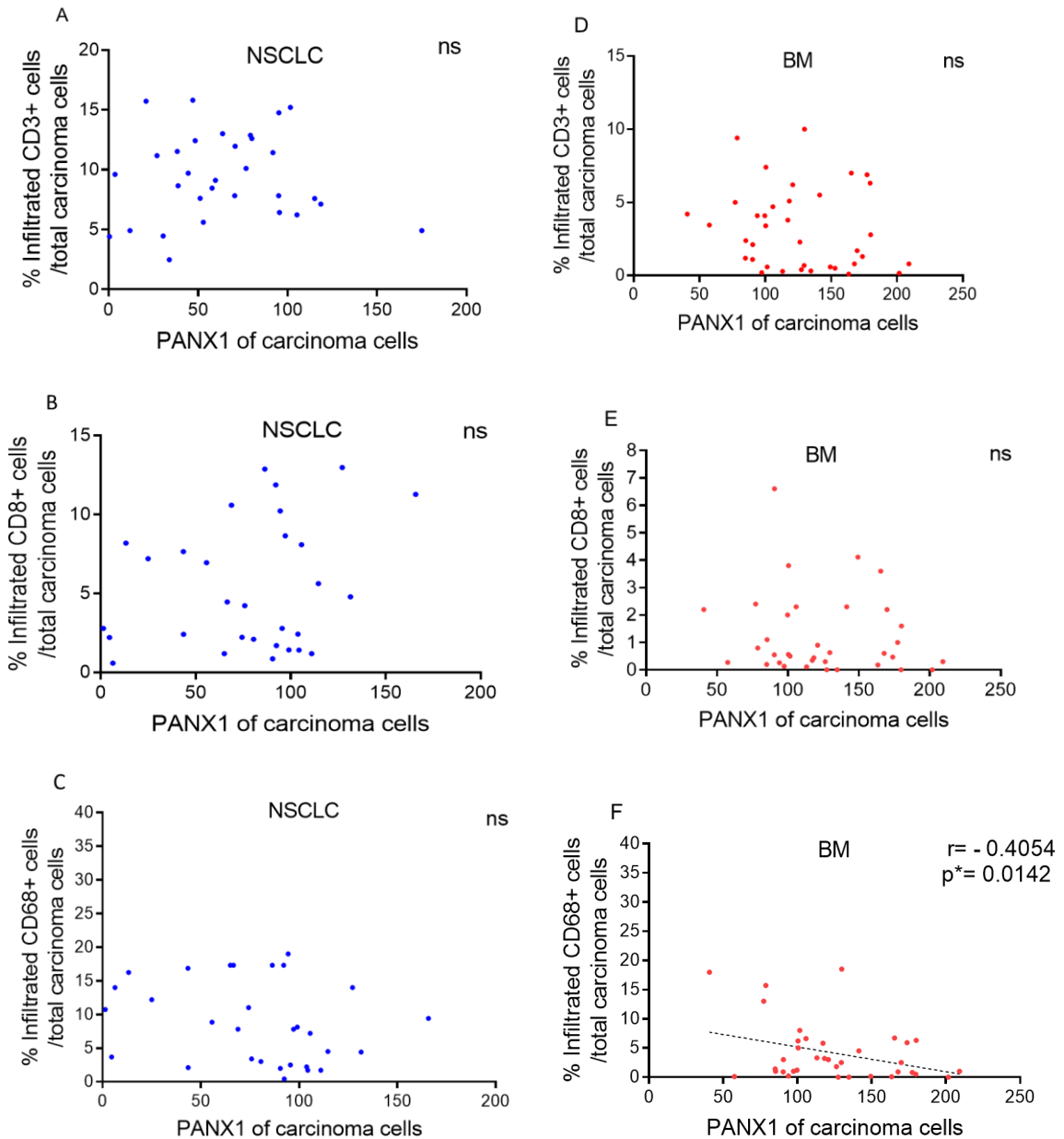
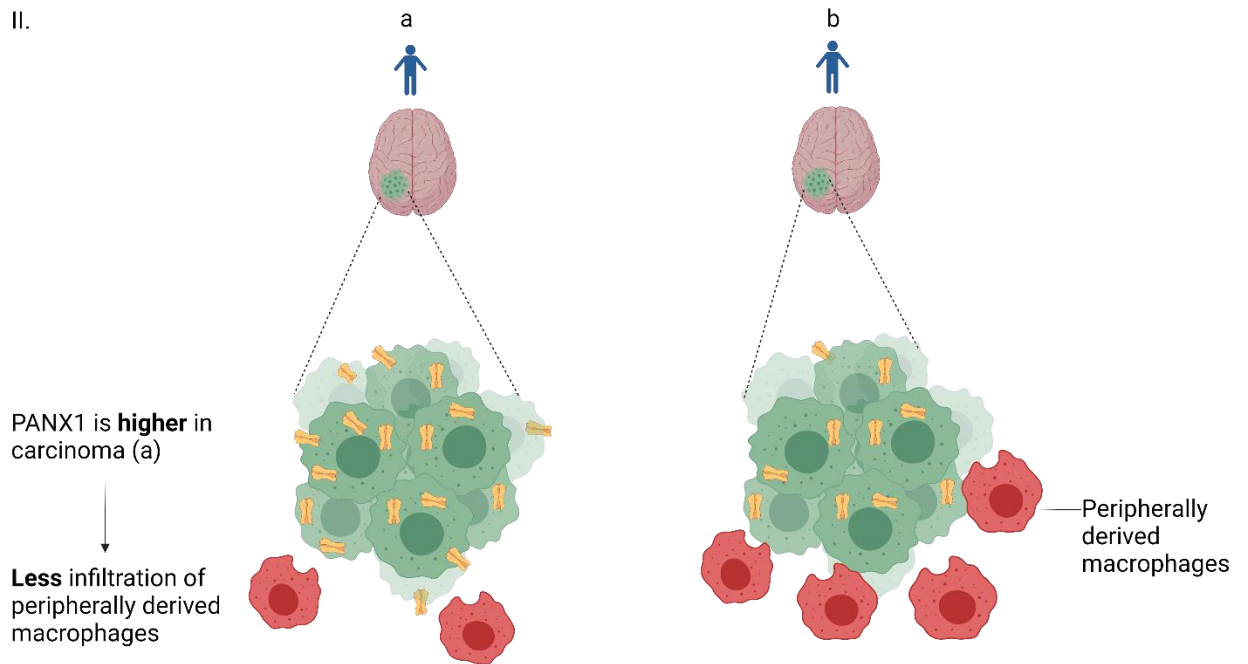
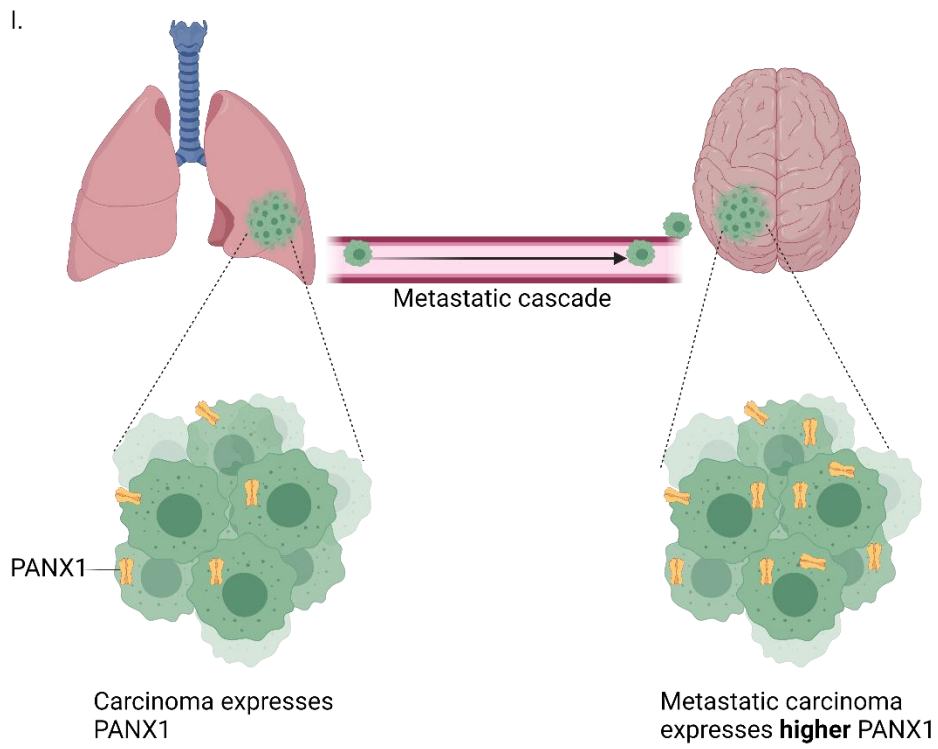


**Figure 12. PANX1 of lung carcinoma cells is associated with less infiltration of blood-derived macrophages in BM.** **A, B & C** Scatter Plot shows no statistical correlation between PANX1 levels of carcinoma cells and the percentage of CD3+, CD8+, or CD68+ cell infiltrations in NSCLC. **D&E** Scatter plots between PANX1 levels of carcinoma cells and the percentage of CD3+, CD8+, CD68+ cell infiltrations in BM. There was no significant correlation between PANX1 levels and the infiltration of CD3+ or CD8+ cells. **F** Scatter Plot between CD68+ cells infiltration and PANX1 levels of lung carcinoma cells in BM shows a significantly negative correlation, where (Pearson  $r = -0.40$ ) and ( $*P = 0.0142$ ), indicating that a high- PANX1 level of lung carcinoma cells is associated with a lower infiltration of blood-derived macrophages in BM.



## Graphical Summary



## **Section 4: Discussion**

PANX1 has not been characterized in NSCLCs nor brain metastasis of patient-derived specimens at a protein level. Brain metastases are primarily originated from NSCLC and represent the leading cause of cancer-associated death. Although clinical trials showed a promising effect of immune checkpoint inhibitors in asymptomatic brain metastases due to NSCLC, there remains a robust demand for new biomarkers that effectively anticipate response to ICIs<sup>166</sup>. Furthermore, a PANX1 role has not been identified in the immune landscape in tumors. Here, we investigated the expression of PANX1 and immune profiling in primary NSCLCs and matched brain metastases. For the first time, we demonstrated that (i) brain metastases derived from NSCLCs exhibit higher expression of PANX1, (ii) less density of CD3+, CD8+, and CD68+ immune cell infiltrations in comparison to primary NSCLC, and (iii) higher PANX1 in brain metastases was associated with less infiltration of blood-derived macrophages. Our results suggest that PANX1 plays a role in lung carcinoma progression and immune profiling of metastatic lung carcinoma.

The role of PANX1 in tumorigenesis and metastasis progression has been documented in different malignancies. PANX1 has been, for instance, found across three stages of patient-derived melanoma tumors- in primary sites of melanoma, metastatic lymph nodes, and distal metastasis sites<sup>131</sup>. PANX1 expression was higher in melanoma tumors than normal skin without a significant difference among the tumor stages. In melanoma cell lines, PANX1-depleted cells had less growth and migration compared to PANX1-abundant cells<sup>131</sup>. In a

chicken embryo model, implanted BL6 mouse melanoma tumors derived from PANX1 knockdown cells were significantly smaller, contained less blood, and metastasized with less number of mouse cells to the liver compared to those derived from control cells<sup>132</sup>. The human melanoma cells with PANX1 blocked by pharmacological inhibitors showed reduced invasiveness in the primary tumors, although distant metastasis could not be evaluated<sup>131</sup>. Nonetheless, in hepatocellular carcinoma (HCC), PANX1 expression levels were positively correlated with the TNM classification of malignant tumors in human-derived specimens<sup>135</sup>. Patients with high PANX1 expression in tumors displayed a more advanced disease state than patients with low expression of PANX in tumors. Additionally, PANX1 overexpression significantly induced metastasis in HCC cell lines and inducible mice by promoting EMT through AKT signaling<sup>135</sup>. In breast cancer, a gain-of-function mutation of PANX1 channels enhances the metastasis capability of tumor cells to disseminate to the lung, bone, and liver in a mouse model<sup>107</sup>. Pharmacological inhibition of PANX1 in breast cancer cells or genetic deletion of PANX1 retrogressed the EMT phenotype<sup>133</sup>.

The TME is considered a fundamental regulator of cancer progression, and Adenosine triphosphate (ATP) is one of the critical biological compounds of TME<sup>167</sup>. PANX1 may enhance the progression of lung carcinoma through ATP release in association with other purinergic receptors<sup>168</sup>. However, PANX1 distributed intracellularly in NSCLCs and brain metastases in our cohort, suggesting a different role than PANX1 at the cell membrane. PANX1 at a cell membrane is involved in the conductance of ATP and molecules that are less

than (1) kDa under pathophysiological conditions. Intracellular PANX1, however, could be involved in WNT/  $\beta$ -catenin signaling pathway<sup>160</sup>.  $\beta$ -catenin is essential for the progression of mutated EGFR lung carcinoma, accounting for approximately 20% of mutations in NSCLC<sup>14</sup>.  $\beta$ -catenin, the main component of WNT/TCF signaling, additionally mediates lung adenocarcinoma metastasis to the brain<sup>169</sup>. We found that  $\beta$ -catenin expression is higher in brain metastases in comparison to NSCLC, demonstrating the role of  $\beta$ -catenin in the progression of advanced lung carcinoma in association with PANX1. Previously, it was shown that PANX1 and  $\beta$ -catenin interact to modulate the growth and metabolism of melanoma cell lines<sup>160</sup>. Nonetheless, PANX1/  $\beta$ -catenin interaction may still exist in these carcinoma cells since they co-express both proteins that have been shown to interact directly. Furthermore, intracellular PANX1 could locate in the ER, evoking calcium release from internal stores in prostate cancer cells<sup>170</sup>, and we know that  $\text{Ca}^{2+}$  plays a significant role in metastasis<sup>171</sup>. Therefore, it is possible that the signaling that occurs via intracellular PANX1 has more to do with calcium signaling than with other functions at the cell surface. Further, studies have linked PANX1 and metastasis through the EMT pathway, where inhibiting PANX1 channels pharmacologically or genetically led to a decrease of vimentin,  $\beta$ -catenin, snail, and slug<sup>133,135</sup>. PANX1 has also been linked to metastasis by activating the ERK1/2 pathway in I-10 testicular cell lines<sup>134</sup>. Therefore, intracellular PANX1 could be essential for the metastasis cascade through activating signaling pathways, such as  $\text{Ca}^{+2}$  signaling in the ER<sup>170</sup>, EMT pathway<sup>135</sup>, AKT/PI3K pathway<sup>134</sup>, or the Wnt / $\beta$ -catenin pathway<sup>160</sup>.

The level of PANX1 in primary NSCLCs did not correlate with the metastatic time interval. However, there was a tendency of lung carcinoma cases with high levels of PANX1 to metastasize to the brain earlier, particularly with less aggressive cases. Here, we found that high PANX1 in 11 cases with  $\geq 20$ -month of metastatic duration needed less time to metastasize to the brain. Nonetheless, the sample number needs to be more significant to conclude. Aggressive mutations could drive the metastasis progression in the cases (n=31) with 20 months > time intervals.

Evaluating the immune profile in brain metastases is essential in light of immune checkpoint blockade treatments, which have shown efficacy in clinical trials using anti-PD-1/PDL-1 antibodies in asymptomatic brain metastasis patients with primary lung carcinoma<sup>166</sup>. Our study found that the infiltration levels of CD3/CD8/CD68+ cells in primary lung carcinoma were higher than in brain metastases. Primary lung tumors have more immune infiltration than their metastases in the brain since they have been established longer and have developed more immunological mechanisms. However, neither the density of CD8+ immune cells nor the density of CD68+ immune cells in primary NSCLC was correlated with the metastatic time interval.

Our study found that primary lung carcinoma cells have higher expression of PD-L1 than metastatic lung carcinoma cells in the brain by IHC assessment. PANX1 was not correlated with PD-L1 expression in NSCLC nor in brain metastasis. We additionally revealed that PANX1 expression of metastatic lung carcinoma in the brain was associated with less infiltration of macrophages. PANX1 channel

activity has been linked to the recruitment of immune cells through ATP signaling in non-tumor conditions<sup>122,172</sup>. However, the role of PANX1 in immune status in a cancer context has not yet been explored. Our observation could be attributed to several factors, such as that PANX1 channels are more intercellular than at a cell membrane in lung carcinoma cells. Therefore, the theory of PANX1 releasing ATP as a signal “find me” for immune cells may have less contribution in the malignancy context.

Additionally, macrophages are physiologically subtyped into M1 (pro-inflammatory) and M2 (anti-inflammatory); therefore, it could be related to the pathophysiology of a macrophage phenotype. On the other hand, macrophages also express PANX1<sup>173</sup>, which might play an anti-inflammatory role in metastatic lung carcinoma cells in the brain. Further studies on a different model are needed to assess the interplay between PANX1 and macrophages in brain metastases derived from NSCLC.

In immunotherapy applications, PD-L1 of tumor cells was utilized as predictive markers for assessing the efficacy of ICIs<sup>143</sup>. Additionally, PD-L1 of TME has recently been considered an additional component to evaluate the PD-L1 status<sup>143</sup>. In NSCLC, the predominant immune cell type that expresses PD-L1 is CD68 macrophages<sup>162</sup>. Interestingly, recent studies documented that the level of PD-L1 in macrophages is correlated with longer OS in melanoma<sup>151</sup> and NSCLC patients<sup>162</sup> treated with anti-PD-1/PD-L1 therapies. Hence, pharmacological blockade of PANX1 channels could play a reverse effect and attract more macrophages in brain metastases and subsequently have greater expression of

PD-L1 in TME, which may enhance the effectiveness of ICIs in advanced NSCLC. Further studies are required to evaluate this notion.

### **Limitation of the study and future directions**

This study investigated the significance of PANX1 in the progression of brain metastases derived from NSCLC, but it still has some limitations. Although high expression of PANX1 in primary lung carcinoma can predict a higher level of PANX1 in brain metastases, it lacks clinical applications, such as predicting the metastatic time interval. Additionally, despite the confirmation that PANX1 is upregulated in brain metastases and correlated with less infiltration of macrophages, we did not provide the detailed mechanism nor identify the subset of macrophages in brain metastases. Further, immune markers often have a high level of heterogeneity; therefore, accurate representation of the tumor and the TME is essential<sup>151</sup>. For our study, we used three nonadjacent TMA cores for each patient to minimize sampling errors, but this still represents a very small percentage of a standard tissue section.

Immunohistochemistry in pathological anatomy and digital pathology supports subjective perception and directly corresponds to the experience of the hands and the expertise in interpreting the results<sup>174,175</sup>. Therefore, immunostaining methods can be variable and may present significant bias. Hence, its outcomes must be interpreted with caution.



However, the study unravels the role of PANX1 in the progression of metastatic NSCLC to the brain and highlights the association of NSCLC PANX1 with the immune landscape in brain metastasis, paving a new avenue for a treatment approach that may enhance the efficacy of ICIs. Future directions of our study would investigate the mechanism of the cross-talk between PANX1 of lung carcinoma cells and blood-derived macrophages in brain metastasis in a mouse model, where the levels of PANX1 in different cell types could be modified, and the use of PANX1 blockers could be evaluated.

## References

1. Bray, F. *et al.* Global cancer statistics 2018: GLOBOCAN estimates of incidence and mortality worldwide for 36 cancers in 185 countries. *CA. Cancer J. Clin.* **68**, 394–424 (2018).
2. Travis, W. D. *et al.* The 2015 World Health Organization Classification of Lung Tumors: Impact of Genetic, Clinical and Radiologic Advances Since the 2004 Classification. *J. Thorac. Oncol. Off. Publ. Int. Assoc. Study Lung Cancer* **10**, 1243–1260 (2015).
3. Davidson, M. R., Gazdar, A. F. & Clarke, B. E. The pivotal role of pathology in the management of lung cancer. *J. Thorac. Dis.* **5**, (2013).
4. Langer, C. J., Besse, B., Gualberto, A., Brambilla, E. & Soria, J.-C. The Evolving Role of Histology in the Management of Advanced Non–Small-Cell Lung Cancer. *J. Clin. Oncol.* **28**, 5311–5320 (2010).
5. Lu, Y. *et al.* Evidence That SOX2 Overexpression Is Oncogenic in the Lung. *PLoS ONE* **5**, e11022 (2010).
6. Dang, A.-T. H. *et al.* Actionable Mutation Profiles of Non-Small Cell Lung Cancer patients from Vietnamese population. *Sci. Rep.* **10**, 2707 (2020).
7. Davies, H. *et al.* Mutations of the BRAF gene in human cancer. *Nature* **417**, 949–954 (2002).
8. Santos, E. *et al.* Malignant activation of a K-ras oncogene in lung carcinoma but not in normal tissue of the same patient. *Science* **223**, 661–664 (1984).
9. Paez, J. G. *et al.* EGFR Mutations in Lung Cancer: Correlation with Clinical Response to Gefitinib Therapy. *Science* **304**, 1497–1500 (2004).
10. Pao, W. *et al.* EGF receptor gene mutations are common in lung cancers from “never smokers” and are associated with sensitivity of tumors to gefitinib and erlotinib. *Proc. Natl. Acad. Sci.* **101**, 13306–13311 (2004).
11. Shepherd, F. A., Hirsh, V., Smylie, M., Findlay, B. & Santabárbara, P. Erlotinib in Previously Treated Non–Small-Cell Lung Cancer. *N. Engl. J. Med.* **10** (2005).
12. Lynch, T. J., Okimoto, R. A., Supko, J. G. & Settleman, J. Activating Mutations in the Epidermal Growth Factor Receptor Underlying Responsiveness of Non–Small-Cell Lung Cancer to Gefitinib. *N. Engl. J. Med.* **11** (2004).
13. Chen, X. *et al.* Genetic profile of non-small cell lung cancer (NSCLC): A hospital-based survey in Jinhua. *Mol. Genet. Genomic Med.* **8**, e1398 (2020).

14. Nakayama, S. *et al.*  $\beta$ -Catenin Contributes to Lung Tumor Development Induced by EGFR Mutations. *Cancer Res.* **74**, 5891–5902 (2014).
15. Achrol, A. S. *et al.* Brain metastases. *Nat. Rev. Dis. Primer* **5**, 1–26 (2019).
16. Tsukada, Y., Fouad, A., Pickren, J. W. & Lane, W. W. Central nervous system metastasis from breast carcinoma. Autopsy study. *Cancer* **52**, 2349–2354 (1983).
17. Berghoff, A. S. *et al.* Descriptive statistical analysis of a real life cohort of 2419 patients with brain metastases of solid cancers. *ESMO Open* **1**, e000024 (2016).
18. Sperduto, P. W. *et al.* Diagnosis-Specific Prognostic Factors, Indexes, and Treatment Outcomes for Patients With Newly Diagnosed Brain Metastases: A Multi-Institutional Analysis of 4,259 Patients. *Int. J. Radiat. Oncol.* **77**, 655–661 (2010).
19. Eichler, A. F. *et al.* The biology of brain metastases—translation to new therapies. *Nat. Rev. Clin. Oncol.* **8**, 344 (2011).
20. Martin, A. M. *et al.* Brain Metastases in Newly Diagnosed Breast Cancer: A Population-Based Study. *JAMA Oncol.* **3**, 1069–1077 (2017).
21. Toyokawa, G., Seto, T., Takenoyama, M. & Ichinose, Y. Insights into brain metastasis in patients with ALK+ lung cancer: is the brain truly a sanctuary? *Cancer Metastasis Rev.* **34**, 797–805 (2015).
22. Steeg, P. S., Camphausen, K. A. & Smith, Q. R. Brain metastases as preventive and therapeutic targets. *Nat. Rev. Cancer* **11**, 352–363 (2011).
23. Nieder, C., Yobuta, R. & Mannsåker, B. Patterns of Treatment and Outcome in Patients With 20 or More Brain Metastases. *In Vivo* **33**, 173–176 (2019).
24. Barnholtz-Sloan, J. S. *et al.* Incidence Proportions of Brain Metastases in Patients Diagnosed (1973 to 2001) in the Metropolitan Detroit Cancer Surveillance System. *J. Clin. Oncol.* (2016) doi:10.1200/JCO.2004.12.149.
25. Hung, M.-H. *et al.* Effect of Age and Biological Subtype on the Risk and Timing of Brain Metastasis in Breast Cancer Patients. *PLoS ONE* **9**, e89389 (2014).
26. Wicha, M. S., Liu, S. & Dontu, G. Cancer stem cells: an old idea—a paradigm shift. *Cancer Res.* **66**, 1883–1890 (2006).

27. Fischer, K. R. *et al.* Epithelial-to-mesenchymal transition is not required for lung metastasis but contributes to chemoresistance. *Nature* **527**, 472–476 (2015).
28. Chambers, A. F., Groom, A. C. & MacDonald, I. C. Dissemination and growth of cancer cells in metastatic sites. *Nat. Rev. Cancer* **2**, 563–572 (2002).
29. Kienast, Y. *et al.* Real-time imaging reveals the single steps of brain metastasis formation. *Nat. Med.* **16**, 116–122 (2010).
30. Lyle, L. T. *et al.* Alterations in Pericyte Subpopulations Are Associated with Elevated Blood–Tumor Barrier Permeability in Experimental Brain Metastasis of Breast Cancer. *Clin. Cancer Res.* **22**, 5287–5299 (2016).
31. Boire, A. *et al.* Complement Component 3 Adapts the Cerebrospinal Fluid for Leptomeningeal Metastasis. *Cell* **168**, 1101–1113.e13 (2017).
32. Heyn, C. *et al.* In vivo MRI of cancer cell fate at the single-cell level in a mouse model of breast cancer metastasis to the brain. *Magn. Reson. Med.* **56**, 1001–1010 (2006).
33. Loriger, M. & Felding-Habermann, B. Capturing changes in the brain microenvironment during initial steps of breast cancer brain metastasis. *Am. J. Pathol.* **176**, 2958–2971 (2010).
34. Waqar, S. N. *et al.* Non–small-cell Lung Cancer With Brain Metastasis at Presentation. *Clin. Lung Cancer* **19**, e373–e379 (2018).
35. Yousefi, M. *et al.* Lung cancer-associated brain metastasis: Molecular mechanisms and therapeutic options. *Cell. Oncol.* **40**, 419–441 (2017).
36. Matsumoto, S. *et al.* Prevalence and specificity of LKB1 genetic alterations in lung cancers. *Oncogene* **26**, 5911–5918 (2007).
37. Ji, M. *et al.* PD-1/PD-L1 pathway in non-small-cell lung cancer and its relation with EGFR mutation. *J. Transl. Med.* **13**, 5 (2015).
38. Shi, W. & Dicker, A. P. CNS Metastases in Patients With Non–Small-Cell Lung Cancer and *ALK* Gene Rearrangement. *J. Clin. Oncol.* **34**, 107–109 (2016).
39. Wang, H. *et al.* Genes associated with increased brain metastasis risk in non–small cell lung cancer: Comprehensive genomic profiling of 61 resected brain metastases versus primary non–small cell lung cancer (Guangdong Association Study of Thoracic Oncology 1036). *Cancer* **125**, 3535–3544 (2019).
40. C, V. *et al.* EGFR, KRAS, BRAF, and HER-2 molecular status in brain metastases from 77 NSCLC patients. *Cancer Med.* **2**, 296–304 (2013).
41. Gow, C.-H. *et al.* Comparison of epidermal growth factor receptor mutations between primary and corresponding metastatic tumors in tyrosine

- kinase inhibitor-naive non-small-cell lung cancer. *Ann. Oncol. Off. J. Eur. Soc. Med. Oncol.* **20**, 696–702 (2009).
42. Kamila, W.-K. *et al.* EGFR activating mutations detected by different PCR techniques in Caucasian NSCLC patients with CNS metastases: short report. *Clin. Exp. Metastasis* **30**, 1063–1071 (2013).
43. Munfus-McCray, D. *et al.* EGFR and KRAS mutations in metastatic lung adenocarcinomas. *Hum. Pathol.* **42**, 1447–1453 (2011).
44. Matsumoto, S. *et al.* Frequent EGFR mutations in brain metastases of lung adenocarcinoma. *Int. J. Cancer* **119**, 1491–1494 (2006).
45. You, H., Baluszek, S. & Kaminska, B. Immune Microenvironment of Brain Metastases—Are Microglia and Other Brain Macrophages Little Helpers? *Front. Immunol.* **10**, 1941 (2019).
46. Galea, I., Bechmann, I. & Perry, V. H. What is immune privilege (not)? *Trends Immunol.* **28**, 12–18 (2007).
47. Hudson, L. C., Bragg, D. C., Tompkins, M. B. & Meeker, R. B. Astrocytes and microglia differentially regulate trafficking of lymphocyte subsets across brain endothelial cells. *Brain Res.* **1058**, 148–160 (2005).
48. Fridman, W. H., Pagès, F., Sautès-Fridman, C. & Galon, J. The immune contexture in human tumours: impact on clinical outcome. *Nat. Rev. Cancer* **12**, 298–306 (2012).
49. Graeber, M. B. & Streit, W. J. Microglia: biology and pathology. *Acta Neuropathol. (Berl.)* **119**, 89–105 (2010).
50. Osswald, M. & Winkler, F. Insights into cell-to-cell and cell-to-blood-vessel communications in the brain: in vivo multiphoton microscopy. *Cell Tissue Res.* **352**, 149–159 (2013).
51. Berghoff, A. S. *et al.* Programmed death ligand 1 expression and tumor-infiltrating lymphocytes in glioblastoma. *Neuro-Oncol.* **17**, 1064–1075 (2015).
52. Ojalvo, L. S., Whittaker, C. A., Condeelis, J. S. & Pollard, J. W. Gene Expression Analysis of Macrophages That Facilitate Tumor Invasion Supports a Role for Wnt-Signaling in Mediating Their Activity in Primary Mammary Tumors. *J. Immunol. Baltim. Md 1950* **184**, 702–712 (2010).
53. Bowman, R. L. *et al.* Macrophage Ontogeny Underlies Differences in Tumor-Specific Education in Brain Malignancies. *Cell Rep.* **17**, 2445–2459 (2016).
54. Bennett, M. L. *et al.* New tools for studying microglia in the mouse and human CNS. *Proc. Natl. Acad. Sci.* **113**, E1738–E1746 (2016).

55. Lu, W. *et al.* Genomic landscape of the immune microenvironments of brain metastases in breast cancer. *J. Transl. Med.* **18**, 327 (2020).
56. Berghoff, A. S. *et al.* Density of tumor-infiltrating lymphocytes correlates with extent of brain edema and overall survival time in patients with brain metastases. *Oncolimmunology* **5**, e1057388 (2016).
57. Berghoff, A. S. *et al.* Density of tumor-infiltrating lymphocytes correlates with extent of brain edema and overall survival time in patients with brain metastases. *Oncolimmunology* **5**, e1057388 (2016).
58. Harter, P. N. *et al.* Distribution and prognostic relevance of tumor-infiltrating lymphocytes (TILs) and PD-1/PD-L1 immune checkpoints in human brain metastases. *Oncotarget* **6**, 40836 (2015).
59. Jindal, V. & Gupta, S. Expected Paradigm Shift in Brain Metastases Therapy—Immune Checkpoint Inhibitors. *Mol. Neurobiol.* **55**, 7072–7078 (2018).
60. Sharpe, A. H., Wherry, E. J., Ahmed, R. & Freeman, G. J. The function of programmed cell death 1 and its ligands in regulating autoimmunity and infection. *Nat. Immunol.* **8**, 239–245 (2007).
61. Pardoll, D. M. The blockade of immune checkpoints in cancer immunotherapy. *Nat. Rev. Cancer* **12**, 252–264 (2012).
62. Dong, H. *et al.* Tumor-associated B7-H1 promotes T-cell apoptosis: a potential mechanism of immune evasion. *Nat. Med.* **8**, 793–800 (2002).
63. Zou, W., Wolchok, J. D. & Chen, L. PD-L1 (B7-H1) and PD-1 pathway blockade for cancer therapy: Mechanisms, response biomarkers, and combinations. *Sci. Transl. Med.* **8**, 328rv4-328rv4 (2016).
64. Téglási, V. *et al.* Evaluating the significance of density, localization, and PD-1/PD-L1 immunopositivity of mononuclear cells in the clinical course of lung adenocarcinoma patients with brain metastasis. *Neuro-Oncol.* **19**, 1058–1067 (2017).
65. Mansfield, A. S. *et al.* Temporal and spatial discordance of programmed cell death-ligand 1 expression and lymphocyte tumor infiltration between paired primary lesions and brain metastases in lung cancer. *Ann. Oncol.* **27**, 1953–1958 (2016).
66. Mansfield, A. S. *et al.* Contraction of T cell richness in lung cancer brain metastases. *Sci. Rep.* **8**, 2171 (2018).
67. Dong, J., Li, B., Lin, D., Zhou, Q. & Huang, D. Advances in Targeted Therapy and Immunotherapy for Non-small Cell Lung Cancer Based on Accurate Molecular Typing. *Front. Pharmacol.* **10**, (2019).

68. Soffiatti, R., Ahluwalia, M., Lin, N. & Rudà, R. Management of brain metastases according to molecular subtypes. *Nat. Rev. Neurol.* **16**, 557–574 (2020).
69. Gandhi, L. *et al.* Pembrolizumab plus Chemotherapy in Metastatic Non–Small-Cell Lung Cancer. *N. Engl. J. Med.* **378**, 2078–2092 (2018).
70. Horn, L. *et al.* First-Line Atezolizumab plus Chemotherapy in Extensive-Stage Small-Cell Lung Cancer. *N. Engl. J. Med.* **379**, 2220–2229 (2018).
71. Fehrenbacher, L. *et al.* Updated Efficacy Analysis Including Secondary Population Results for OAK: A Randomized Phase III Study of Atezolizumab versus Docetaxel in Patients with Previously Treated Advanced Non–Small Cell Lung Cancer. *J. Thorac. Oncol.* **13**, 1156–1170 (2018).
72. Goldberg, S. B. *et al.* Pembrolizumab for management of patients with NSCLC and brain metastases: long-term results and biomarker analysis from a non-randomised, open-label, phase 2 trial. *Lancet Oncol.* **21**, 655–663 (2020).
73. Feng, L., Cai, Y., Zhu, M., Xing, L. & Wang, X. The yin and yang functions of extracellular ATP and adenosine in tumor immunity. *Cancer Cell Int.* **20**, 110 (2020).
74. Panchina, Y. *et al.* A ubiquitous family of putative gap junction molecules. *Curr. Biol.* **10**, R473–R474 (2000).
75. Penuela, S., Gehi, R. & Laird, D. W. The biochemistry and function of pannexin channels. *Biochim. Biophys. Acta BBA - Biomembr.* **1828**, 15–22 (2013).
76. D’hondt, C. *et al.* Pannexin channels in ATP release and beyond: an unexpected rendezvous at the endoplasmic reticulum. *Cell. Signal.* **23**, 305–316 (2011).
77. Sosinsky, G. E. *et al.* Pannexin channels are not gap junction hemichannels. *Channels* **5**, 193–197 (2011).
78. Baranova, A. *et al.* The mammalian pannexin family is homologous to the invertebrate innexin gap junction proteins. *Genomics* **83**, 706–716 (2004).
79. Mr, Y. & Jr, S. M. Gap junctional proteins of animals: the innexin/pannexin superfamily. *Prog. Biophys. Mol. Biol.* **94**, 5–14 (2007).
80. Penuela, S. *et al.* Pannexin 1 and pannexin 3 are glycoproteins that exhibit many distinct characteristics from the connexin family of gap junction proteins. *J. Cell Sci.* **120**, 3772–3783 (2007).

81. Boassa, D. *et al.* Pannexin1 Channels Contain a Glycosylation Site That Targets the Hexamer to the Plasma Membrane \*. *J. Biol. Chem.* **282**, 31733–31743 (2007).
82. Bruzzone, R., White, T. W. & Paul, D. L. Connections with connexins: the molecular basis of direct intercellular signaling. *Eur. J. Biochem.* **238**, 1–27 (1996).
83. Deng, Z. *et al.* Cryo-EM structures of the ATP release channel pannexin 1. *Nat. Struct. Mol. Biol.* **27**, 373–381 (2020).
84. Bhalla-Gehi, R., Penuela, S., Churko, J. M., Shao, Q. & Laird, D. W. Pannexin1 and pannexin3 delivery, cell surface dynamics, and cytoskeletal interactions. *J. Biol. Chem.* **285**, 9147–9160 (2010).
85. Penuela, S., Bhalla, R., Nag, K. & Laird, D. W. Glycosylation regulates pannexin intermixing and cellular localization. *Mol. Biol. Cell* **20**, 4313–4323 (2009).
86. Baranova, A. *et al.* The mammalian pannexin family is homologous to the invertebrate innexin gap junction proteins. *Genomics* **83**, 706–716 (2004).
87. Dw, L. Life cycle of connexins in health and disease. *Biochem. J.* **394**, 527–543 (2006).
88. Boassa, D., Qiu, F., Dahl, G. & Sosinsky, G. Trafficking dynamics of glycosylated pannexin1 proteins. *Cell Commun. Adhes.* **15**, 119–132 (2008).
89. Goodenough, D. A., Goliger, J. A. & Paul, D. L. Connexins, connexons, and intercellular communication. *Annu. Rev. Biochem.* **65**, 475–502 (1996).
90. Boassa, D., Qiu, F., Dahl, G. & Sosinsky, G. TRAFFICKING DYNAMICS OF GLYCOSYLATED PANNEXIN1 PROTEINS. *Cell Commun. Adhes.* **15**, 119–132 (2008).
91. Iwamoto, T. *et al.* Pannexin 3 Regulates Intracellular ATP/cAMP Levels and Promotes Chondrocyte Differentiation. *J. Biol. Chem.* **285**, 18948–18958 (2010).
92. Cowan, K. N., Langlois, S., Penuela, S., Cowan, B. J. & Laird, D. W. Pannexin1 and Pannexin3 exhibit distinct localization patterns in human skin appendages and are regulated during keratinocyte differentiation and carcinogenesis. *Cell Commun. Adhes.* **19**, 45–53 (2012).
93. Le Vasseur, M., Lelowski, J., Bechberger, J. F., Sin, W.-C. & Naus, C. C. Pannexin 2 protein expression is not restricted to the CNS. *Front. Cell. Neurosci.* **8**, (2014).



94. Dahl, G. & Locovei, S. Pannexin: To gap or not to gap, is that a question? *IUBMB Life* **58**, 409–419 (2006).
95. Chiu, Y.-H., Schappe, M. S., Desai, B. N. & Bayliss, D. A. Revisiting multimodal activation and channel properties of Pannexin 1. *J. Gen. Physiol.* **150**, 19–39 (2018).
96. Jin, Q. *et al.* Cryo-EM structures of human pannexin 1 channel. *Cell Res.* **30**, 449–451 (2020).
97. Qu, R. *et al.* Cryo-EM structure of human heptameric Pannexin 1 channel. *Cell Res.* **30**, 446–448 (2020).
98. Ruan *et al.* - 2020 - Structures of human pannexin 1 reveal ion pathways.pdf.
99. Vanden Abeele, F. *et al.* Functional implications of calcium permeability of the channel formed by pannexin 1. *J. Cell Biol.* **174**, 535–546 (2006).
100. Chekeni, F. B. *et al.* Pannexin 1 channels mediate ‘find-me’ signal release and membrane permeability during apoptosis. *Nature* **467**, 863–867 (2010).
101. Bao, L., Locovei, S. & Dahl, G. Pannexin membrane channels are mechanosensitive conduits for ATP. *FEBS Lett.* **572**, 65–68 (2004).
102. Dahl, G. The Pannexin1 membrane channel: distinct conformations and functions. *FEBS Lett.* **592**, 3201–3209 (2018).
103. Pelegrin, P. & Surprenant, A. Pannexin-1 mediates large pore formation and interleukin-1 $\beta$  release by the ATP-gated P2X7 receptor. *EMBO J.* **25**, 5071–5082 (2006).
104. Locovei, S., Wang, J. & Dahl, G. Activation of pannexin 1 channels by ATP through P2Y receptors and by cytoplasmic calcium. *FEBS Lett.* **580**, 239–244 (2006).
105. Silverman, W. R. *et al.* The Pannexin 1 Channel Activates the Inflammasome in Neurons and Astrocytes \*. *J. Biol. Chem.* **284**, 18143–18151 (2009).
106. Sridharan, M. *et al.* Pannexin 1 is the conduit for low oxygen tension-induced ATP release from human erythrocytes. *Am. J. Physiol.-Heart Circ. Physiol.* **299**, H1146–H1152 (2010).
107. Furlow, P. W. *et al.* Mechanosensitive pannexin-1 channels mediate microvascular metastatic cell survival. *Nat. Cell Biol.* **17**, 943–952 (2015).
108. Qiu, F. & Dahl, G. A permeant regulating its permeation pore: inhibition of pannexin 1 channels by ATP. *Am. J. Physiol. Cell Physiol.* **296**, C250-255 (2009).

109. Michalski, K. & Kawate, T. Carbenoxolone inhibits Pannexin1 channels through interactions in the first extracellular loop. *J. Gen. Physiol.* **147**, 165–174 (2016).
110. Sandilos, J. K. *et al.* Pannexin 1, an ATP release channel, is activated by caspase cleavage of its pore-associated C-terminal autoinhibitory region. *J. Biol. Chem.* **287**, 11303–11311 (2012).
111. Jiang, J. X. & Penuela, S. Connexin and pannexin channels in cancer. *BMC Cell Biol.* **17**, S12 (2016).
112. Zappalà, A. *et al.* Expression of pannexin1 in the CNS of adult mouse: Cellular localization and effect of 4-aminopyridine-induced seizures. *Neuroscience* **141**, 167–178 (2006).
113. Ransford, G. A. *et al.* Pannexin 1 Contributes to ATP Release in Airway Epithelia. *Am. J. Respir. Cell Mol. Biol.* **41**, 525–534 (2009).
114. Hanner, F., Lam, L., Nguyen, M. T. X., Yu, A. & Peti-Peterdi, J. Intrarenal localization of the plasma membrane ATP channel pannexin1. *Am. J. Physiol. - Ren. Physiol.* **303**, F1454–F1459 (2012).
115. Qu, Y. *et al.* Pannexin-1 Is Required for ATP Release during Apoptosis but Not for Inflammasome Activation. *J. Immunol.* **186**, 6553–6561 (2011).
116. Wang, J. & Dahl, G. SCAM analysis of Panx1 suggests a peculiar pore structure. *J. Gen. Physiol.* **136**, 515–527 (2010).
117. Qiu, F., Wang, J. & Dahl, G. Alanine substitution scanning of pannexin1 reveals amino acid residues mediating ATP sensitivity. *Purinergic Signal.* **8**, 81–90 (2012).
118. Séror, C. *et al.* Extracellular ATP acts on P2Y2 purinergic receptors to facilitate HIV-1 infection. *J. Exp. Med.* **208**, 1823–1834 (2011).
119. Santiago, M. F. *et al.* Targeting pannexin1 improves seizure outcome. *PLoS One* **6**, e25178 (2011).
120. Khan, M. *et al.* Blocking pannexin1 reduces airway inflammation in a murine model of asthma. *Am. J. Transl. Res.* **12**, 4074–4083 (2020).
121. Sharma, A. K. *et al.* Pannexin-1 channels on endothelial cells mediate vascular inflammation during lung ischemia-reperfusion injury. *Am. J. Physiol. Lung Cell. Mol. Physiol.* **315**, L301–L312 (2018).
122. Lohman, A. W. *et al.* Pannexin 1 channels regulate leukocyte emigration through the venous endothelium during acute inflammation. *Nat. Commun.* **6**, 7965 (2015).

123. Bao, Y., Chen, Y., Ledderose, C., Li, L. & Junger, W. G. Pannexin 1 Channels Link Chemoattractant Receptor Signaling to Local Excitation and Global Inhibition Responses at the Front and Back of Polarized Neutrophils \*. *J. Biol. Chem.* **288**, 22650–22657 (2013).
124. Lemaire, I., Falzoni, S., Zhang, B., Pellegatti, P. & Virgilio, F. D. The P2X7 Receptor and Pannexin-1 Are Both Required for the Promotion of Multinucleated Macrophages by the Inflammatory Cytokine GM-CSF. *J. Immunol.* **187**, 3878–3887 (2011).
125. Schenk, U. *et al.* Purinergic Control of T Cell Activation by ATP Released Through Pannexin-1 Hemichannels. *Sci. Signal.* **1**, ra6–ra6 (2008).
126. Diezmos, E. F. *et al.* Blockade of Pannexin-1 Channels and Purinergic P2X7 Receptors Shows Protective Effects Against Cytokines-Induced Colitis of Human Colonic Mucosa. *Front. Pharmacol.* **9**, (2018).
127. Shoji, K. F., Sáez, P. J., Harcha, P. A., Aguila, H. L. & Sáez, J. C. Pannexin1 channels act downstream of P2X7 receptors in ATP-induced murine T-cell death. *Channels* **8**, 142–156 (2014).
128. Xu, X., Hao, Y., Xiong, S. & He, Z. PANX2 and brain lower grade glioma genesis: A bioinformatic analysis. *Sci. Prog.* **104**, 00368504211011836 (2021).
129. Gao, J. *et al.* Integrative Analysis of Complex Cancer Genomics and Clinical Profiles Using the cBioPortal. *Sci. Signal.* **6**, pl1–pl1 (2013).
130. Uhlen, M. *et al.* Tissue-based map of the human proteome. *Science* **347**, 1260419–1260419 (2015).
131. Freeman, T. J. *et al.* Inhibition of Pannexin 1 Reduces the Tumorigenic Properties of Human Melanoma Cells. *Cancers* **11**, 102 (2019).
132. Penuela, S. *et al.* Loss of pannexin 1 attenuates melanoma progression by reversion to a melanocytic phenotype. *J. Biol. Chem.* **287**, 29184–29193 (2012).
133. Jalaleddine, N. *et al.* Pannexin1 is associated with enhanced epithelial-to-mesenchymal transition in human patient breast cancer tissues and in breast cancer cell lines. *Cancers* **11**, 1967 (2019).
134. Liu, H. *et al.* In vitro effect of Pannexin 1 channel on the invasion and migration of I-10 testicular cancer cells via ERK1/2 signaling pathway. *Biomed. Pharmacother.* **117**, 109090 (2019).
135. Shi, G. *et al.* Panx1 promotes invasion-metastasis cascade in hepatocellular carcinoma. *J. Cancer* **10**, 5681–5688 (2019).

136. Wei, L., Yang, X., Shi, X. & Chen, Y. Pannexin-1 silencing inhibits the proliferation of U87-MG cells. *Mol. Med. Rep.* **11**, 3487–3492 (2015).
137. Boyd-Tressler, A., Penuela, S., Laird, D. W. & Dubyak, G. R. Chemotherapeutic Drugs Induce ATP Release via Caspase-gated Pannexin-1 Channels and a Caspase/Pannexin-1-independent Mechanism. *J. Biol. Chem.* **289**, 27246–27263 (2014).
138. Largo, C. *et al.* Identification of overexpressed genes in frequently gained/amplified chromosome regions in multiple myeloma. *Haematologica* **91**, 184–191 (2006).
139. Lai, C. P. K. *et al.* Tumor-suppressive effects of pannexin 1 in C6 glioma cells. *Cancer Res.* **67**, 1545–1554 (2007).
140. Schalper, K. A., Carvajal-Hausdorf, D. & Oyarzo, M. P. Possible role of hemichannels in cancer. *Front. Physiol.* **5**, (2014).
141. Xiang, X. *et al.* Pannexin 1 inhibits rhabdomyosarcoma progression through a mechanism independent of its canonical channel function. *Oncogenesis* **7**, 1–16 (2018).
142. Havel, J. J., Chowell, D. & Chan, T. A. The evolving landscape of biomarkers for checkpoint inhibitor immunotherapy. *Nat. Rev. Cancer* **19**, 133–150 (2019).
143. Doroshov, D. B. *et al.* PD-L1 as a biomarker of response to immune-checkpoint inhibitors. *Nat. Rev. Clin. Oncol.* **18**, 345–362 (2021).
144. Xu, Z. *et al.* Assessment of tumor mutation burden calculation from gene panel sequencing data. *OncoTargets Ther.* **Volume 12**, 3401–3409 (2019).
145. Salvatore, V. *et al.* The tumor microenvironment promotes cancer progression and cell migration. *Oncotarget* **8**, 9608–9616 (2016).
146. Binnewies, M. *et al.* Understanding the tumor immune microenvironment (TIME) for effective therapy. *Nat. Med.* **24**, 541–550 (2018).
147. Zhang, Y. & Chen, L. Classification of Advanced Human Cancers Based on Tumor Immunity in the MicroEnvironment (TIME) for Cancer Immunotherapy. *JAMA Oncol.* **2**, 1403–1404 (2016).
148. Chiarella, A. M., Ryu, Y. K., Manji, G. A. & Rustgi, A. K. Extracellular ATP and Adenosine in Cancer Pathogenesis and Treatment. *Trends Cancer* **0**, (2021).
149. Su, Y.-C., Hsu, Y.-C. & Chai, C.-Y. Role of TTF-1, CK20, and CK7 immunohistochemistry for diagnosis of primary and secondary lung adenocarcinoma. *Kaohsiung J. Med. Sci.* **22**, 14–19 (2006).

150. Richani, K. *et al.* Tissue microarray: an effective high-throughput method to study the placenta for clinical and research purposes. *J. Matern. Fetal Neonatal Med.* **19**, 509–515 (2006).
151. Toki, M. I. *et al.* High-plex predictive marker discovery for melanoma immunotherapy-treated patients using digital spatial profiling. *Clin. Cancer Res.* **25**, 5503–5512 (2019).
152. Morrison, M. D. *et al.* Identifying candidate biomarkers for pleomorphic adenoma: a case–control study. *Head Neck Pathol.* **13**, 286–297 (2019).
153. Loughrey, M. B. *et al.* Validation of the systematic scoring of immunohistochemically stained tumour tissue microarrays using QuPath digital image analysis. *Histopathology* **73**, 327–338 (2018).
154. Bankhead, P. *et al.* QuPath: Open source software for digital pathology image analysis. *Sci. Rep.* **7**, 1–7 (2017).
155. Coulson-Gilmer, C. *et al.* Stanniocalcin 2 expression is associated with a favourable outcome in male breast cancer. *J. Pathol. Clin. Res.* **4**, 241–249 (2018).
156. Penuela, S. *et al.* Pannexin 1 and pannexin 3 are glycoproteins that exhibit many distinct characteristics from the connexin family of gap junction proteins. *J. Cell Sci.* **120**, 3772–3783 (2007).
157. Chen, C.-H. *et al.* A novel function of YWHAZ/ $\beta$ -catenin axis in promoting epithelial–mesenchymal transition and lung cancer metastasis. *Mol. Cancer Res.* **10**, 1319–1331 (2012).
158. Zhang, D. *et al.* The role of  $\beta$ -catenin in the initiation and metastasis of TA2 mice spontaneous breast cancer. *J. Cancer* **8**, 2114 (2017).
159. De, P. *et al.* Wnt-beta-catenin pathway signals metastasis-associated tumor cell phenotypes in triple negative breast cancers. *Oncotarget* **7**, 43124–43149 (2016).
160. Sayedyahosseini, S. *et al.* Pannexin 1 binds  $\beta$ -catenin to modulate melanoma cell growth and metabolism. *J. Biol. Chem.* **296**, 100478 (2021).
161. Kudo, Y. *et al.* Suppressed immune microenvironment and repertoire in brain metastases from patients with resected non-small-cell lung cancer. *Ann. Oncol.* **30**, 1521–1530 (2019).
162. Liu, Y. *et al.* Immune Cell PD-L1 Colocalizes with Macrophages and Is Associated with Outcome in PD-1 Pathway Blockade Therapy. *Clin. Cancer Res. Off. J. Am. Assoc. Cancer Res.* **26**, 970–977 (2020).

163. Eguren-Santamaria, I. *et al.* PD-1/PD-L1 Blockers in NSCLC Brain Metastases: Challenging Paradigms and Clinical Practice. *Clin. Cancer Res. Off. J. Am. Assoc. Cancer Res.* **26**, 4186–4197 (2020).
164. Vilariño, N., Bruna, J., Bosch-Barrera, J., Valiente, M. & Nadal, E. Immunotherapy in NSCLC patients with brain metastases. Understanding brain tumor microenvironment and dissecting outcomes from immune checkpoint blockade in the clinic. *Cancer Treat. Rev.* **89**, 102067 (2020).
165. Skribek, M. *et al.* Outcome of Patients with NSCLC and Brain Metastases Treated with Immune Checkpoint Inhibitors in a ‘Real-Life’ Setting. *Cancers* **12**, (2020).
166. Harary, M., Reardon, D. A. & Iorgulescu, J. B. Efficacy and safety of immune checkpoint blockade for brain metastases. *CNS Oncol.* **8**, CNS33 (2019).
167. Di Virgilio, F., Sarti, A. C., Falzoni, S., De Marchi, E. & Adinolfi, E. Extracellular ATP and P2 purinergic signalling in the tumour microenvironment. *Nat. Rev. Cancer* **18**, 601–618 (2018).
168. Wicki-Stordeur, L. E. & Swayne, L. A. The emerging Pannexin 1 signalome: a new nexus revealed? *Front. Cell. Neurosci.* **7**, (2014).
169. Nguyen, D. X. *et al.* WNT/TCF signaling through LEF1 and HOXB9 mediates lung adenocarcinoma metastasis. *Cell* **138**, 51–62 (2009).
170. Lee, N. S. *et al.* Focused Ultrasound Stimulates ER Localized Mechanosensitive PANNEXIN-1 to Mediate Intracellular Calcium Release in Invasive Cancer Cells. *Front. Cell Dev. Biol.* **8**, (2020).
171. Prevarskaya, N., Skryma, R. & Shuba, Y. Calcium in tumour metastasis: new roles for known actors. *Nat. Rev. Cancer* **11**, 609–618 (2011).
172. Valdebenito, S., Barreto, A. & Eugenin, E. A. The role of connexin and pannexin containing channels in the innate and acquired immune response. *Biochim. Biophys. Acta* **1860**, 154–165 (2018).
173. Chen, W. *et al.* Enhanced Macrophage Pannexin 1 Expression and Hemichannel Activation Exacerbates Lethal Experimental Sepsis. *Sci. Rep.* **9**, 160 (2019).
174. Leong, A. S.-Y. & Wright, J. The contribution of immunohistochemical staining in tumour diagnosis. *Histopathology* **11**, 1295–1305 (1987).
175. Baidoshvili, A. *et al.* Evaluating the benefits of digital pathology implementation: time savings in laboratory logistics. *Histopathology* **73**, 784–794 (2018).

## **Section 5: Supplementary Figures**

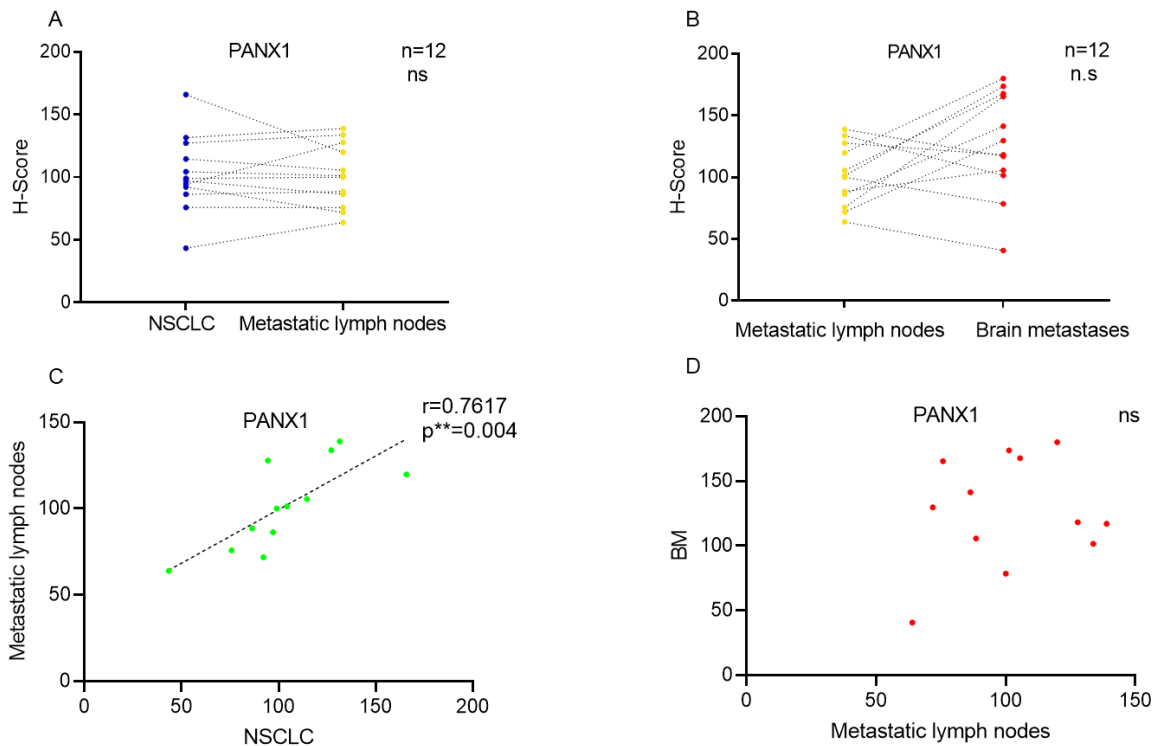


**Figure S.1. Expression of PANX1 had a positive correlation between primary NSCLC and matched metastatic lymph nodes.** Here, we have 12 patients with NSCLC that subsequently metastasized to lymph nodes and the brain. **A** T-test was applied on levels of PANX1 in lung tumors and their metastases in lymph nodes or **B** on PANX1 levels in metastatic lung tumor cells in the lymph nodes and brain and shows no statistical significance. N=12 patients, H-score refers to levels of PANX1. **C** Correlation plot of PANX1 levels between NSCLC and metastatic lymph nodes or **D** between metastatic lymph nodes and brain metastases. PANX1 levels of NSCLC correlated positively and significantly with PANX1 levels of lymph nodes (Pearson  $r=0.76$ ,  $**p=0.04$ ), whereas this correlation was not significant between PANX1 levels of lymph nodes and PANX1 levels of brain metastases.



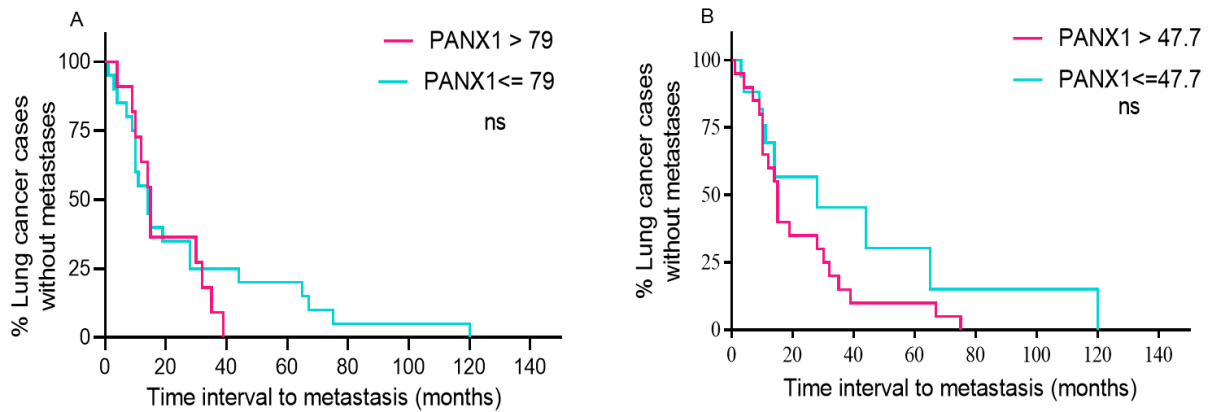


**Figure S.2. Additional thresholds of PANX1 in primary NSCLC determined by quartile and tertile.** Thresholds were applied on a survival curve, where the X-axis indicates metastatic interval (months) to the brain and the Y-axis indicates percentages of primary NSCLC without brain metastases. There was no significant correlation between the PANX1 level of primary NSCLC and metastatic interval to the brain.

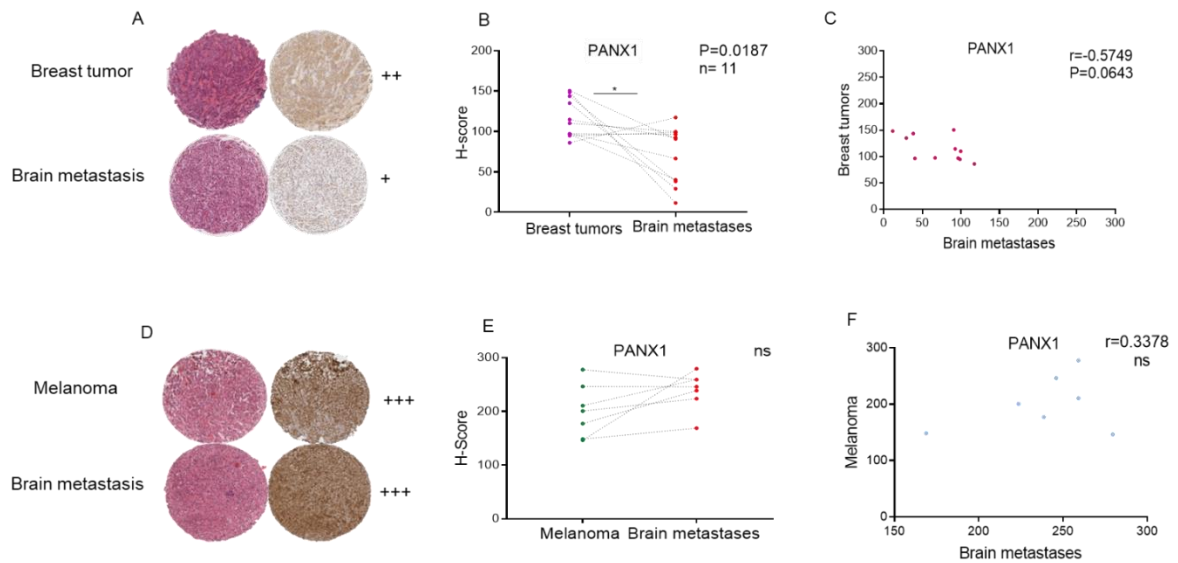


**Figure S.3. Expression of PANX1 in breast tumors or melanoma and matched-brain metastases.** For the breast tumor-brain metastasis cohort, we had 11 patients with breast tumors that metastasized to the brain. **A** IHC using anti-PANX1 antibody on TMA cores of breast tumor and brain metastases. We analyzed the staining intensity of tumor cells in breast tissue cores and brain metastasis cores by QuPath after tracing them based on H&E staining; the staining was more intense in breast tumors (Moderate, ++) compared to brain metastases (weak, +). **B** Statistical quantification of PANX1 levels in breast tumors and brain metastases using t-test; PANX1 levels were significantly higher in breast tumors than matched-brain metastases, where  $p=0.0187$  and H-Score refer to PANX1 levels. **C** Correlation plot of PANX1 between breast tumors and brain metastases. It was a negative correlation with no statistical significance; however, the correlation neared a statistical significance, and increasing the n value might achieve that. Thus, the more PANX1 level is in breast tumors, the less PANX1 level would be in brain metastases. For the melanoma-brain metastasis cohort, seven patients had melanomas and metastasized to the brain. **D** IHC using anti-PANX1 antibody on TMA cores of melanoma-brain metastases; the staining intensity was strong (++++) in melanomas and brain metastases. **E** T-test was applied on levels of PANX1 in melanoma and their metastases in the brain and showed no statistical significance, where  $N=7$  patients, H-score refers to levels of PANX1. **F** correlation plot of PANX1 levels between melanomas and brain metastases shows no statistical correlation, where Pearson  $r=0.3378$ . Images are displayed with a 100- $\mu\text{m}$  resolution.

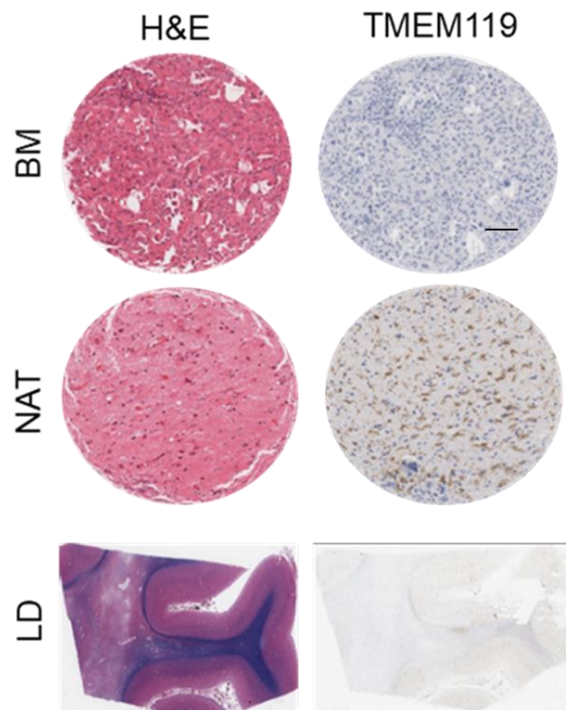


**Figure S.4. Brain metastasis cores are negative for the microglia marker, TMEM119.** Representative images of brain metastasis core stained with H&E and IHC using antibodies raised against TMEM119. Positive controls used are normal brain tissues next to brain metastases (NAT) that have an abundance of microglia and, therefore, were stained intensely with TMEM119 antibody. Another positive control used for the TMEM119 antibody is an autopsy from the leukodystrophy case (LD), which pathologically has a reduction in the microglia population, stained weakly with the TMEM119 antibody. Scale bar= 100  $\mu$ m.

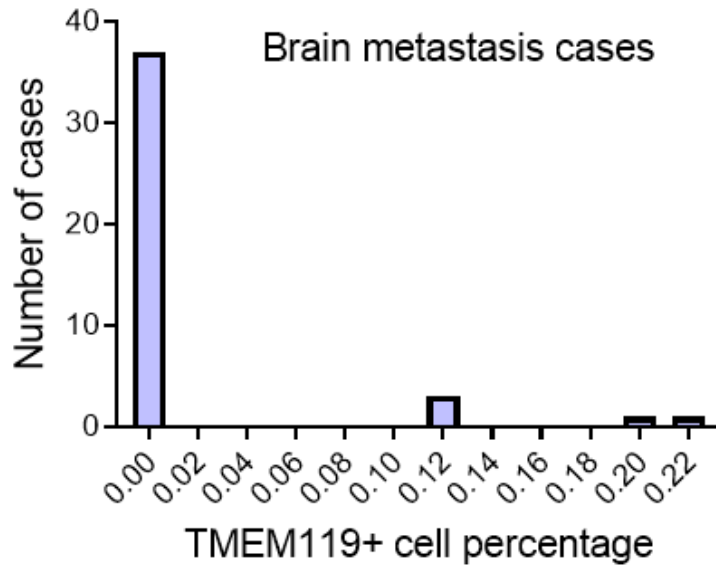


**Figure S.5. Infiltrated CD68+ cells in brain metastasis regions are macrophages derived from blood.** Distribution of BM cases stained with TMEM119 antibody. The majority of BM cases were native for TMEM119 and positive for CD68, indicating that CD68+ are macrophages derived from blood, not microglia.

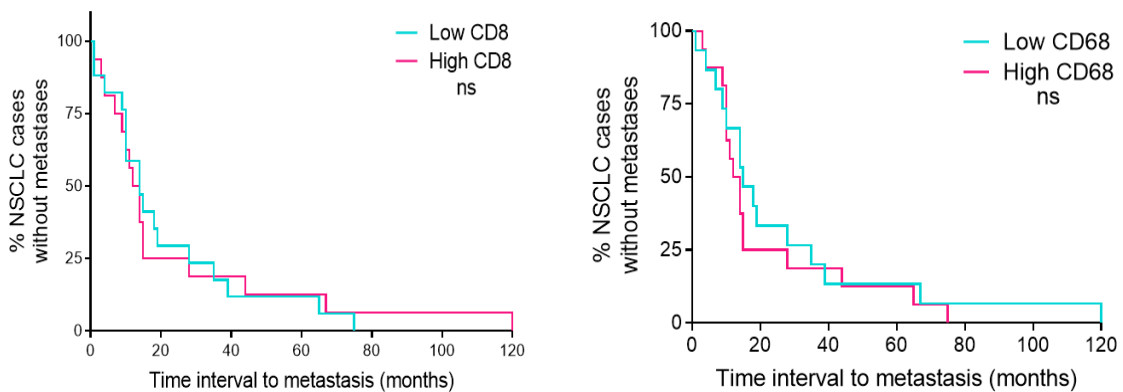


**Figure S.6. There is no correlation between the infiltration level of CD8+ or CD68+ cells and the metastatic time interval.** Survival curve applied on the group of a high density of CD8+/CD68+ cells vs. the group of a low density of CD8+/CD68+ cells in NSCLC. The X-axis indicates time intervals to metastasize to the brain, whereas Y-axis indicates the percentage of NSCLC cases without brain metastases. 'ns' denotes no statistical significance between the two groups.

## Appendix



**Date:** 6 May 2021

**To:** Dr. Qi Zhang

**Project ID:** 111911

**Study Title:** Discovering Predictive Biomarkers of Brain metastatic tumors and rare gliomas

**Application Type:** Continuing Ethics Review (CER) Form

**Review Type:** Delegated

**REB Meeting Date:** 18/May/2021

**Date Approval Issued:** 06/May/2021

**REB Approval Expiry Date:** 22/May/2022

---

Dear Dr. Qi Zhang,

The Western University Research Ethics Board has reviewed the application.

This study, including all currently approved documents, has been re-approved until the

expiry date noted above.

REB members involved in the research project do not participate in the review, discussion or decision.

Western University REB operates in compliance with, and is constituted in accordance with, the requirements of the Tri-Council Policy Statement: Ethical Conduct for Research Involving Humans (TCPS 2); the International Conference on Harmonisation Good Clinical Practice Consolidated Guideline (ICH GCP); Part C, Division 5 of the Food and Drug Regulations; Part 4 of the Natural Health Products Regulations; Part 3 of the Medical Devices Regulations and the provisions of the Ontario Personal Health Information Protection Act (PHIPA 2004) and its applicable regulations. The REB is registered with the U.S. Department of Health & Human Services under the IRB registration number IRB 00000940.

Please do not hesitate to contact us if you have any questions.

Sincerely,

The Office of Human Research Ethics

***Note: This correspondence includes an electronic signature (validation and approval via an online system that is compliant with all regulation).***

## Curriculum Vitae

Rober Abdo

### **Education**

The University of Western Ontario, London, Ontario: 2019-2021

**M.Sc. Candidate, Department of Anatomy and Cell Biology**

Aleppo University Hospital, Aleppo, Syria: 2010-2014

**M.Sc. Candidate, Department of Pediatrics**

The University of Aleppo, Aleppo, Syria: 2004-2010

**M.D.**, Medicine

### **Research-based Contributions**

#### **I. Coursework**

- Anatomy & Cell Biology 9555 – Advanced Topics in Cell and Neurobiology 2019-2020
- Anatomy and Cell Biology 9520/9566 – Research Seminar in Cell and Neurobiology/A Seminar in Professionalism 2019-2021
- Introduction into Biomedical Science 2019
- Communication in the Canadian classroom 2020

#### **II. Teaching Assistance**

Mammalian Histology (ACB 3309) in 2020-2021

#### **III. Conferences, Abstracts, Presentations**

- Terry Fox symposium December 12, 2019



- Abdo R, Soumiya S, Boeters J.L, Johnston D, Penuela S, Zhang Q (2020). Expression of PANX1 in Brain Metastases derived from lung cancer. ACB Research Day 2020. Poster presentation
- Abdo R, Soumiya S, Boeters J.L, Johnston D, Penuela S, Zhang Q (2019). Expression of PANX1 in Brain Metastases. Pathology Research Day 2019, March. Poster presentation
- Abdo R, Soumiya S, Boeters J.L, Johnston D, Penuela S, Zhang Q (2021). Expression of PANX1 in Brain Metastases derived from lung cancer. Pathology Research Day 2021
- Abdo R, Soumiya S, Boeters J.L, Johnston D, Penuela S, Zhang Q (2021). Expression of PANX1 in Brain Metastases derived from lung cancer. London Research Day 2021. Poster presentation

#### **IV. Publications**

- Carolyn Twible, Rober Abdo, and Qi Zhang. Astrocyte role in temporal lobe epilepsy and development of mossy fiber sprouting, *Frontiers in Cellular Neuroscience*, 2021 (under review, Manuscript ID: 725693).

#### **V. Other Contributions**

- I have been working with Dr. Zhang on a project entitled “Transcriptomic Profiles of Lung cancer-brain metastases.” I am involved in constructing tissue microarrays from 44 cases, assisting with selecting the regions of interest (ROIs), and collaborating with

Dr. Cristiana Losef and Dr. Shawn Li in data analysis.

### **Work Experience**

- Teaching Assistant, the University of Western Ontario, Sep 2020 - Apr 2021, London, Ontario, Canada.
- Student Research Assistant, The University of Western Ontario, May 2019 - Sep 2019
- Behavioral Health Coordinator, Mount Hope, Jan 2019 - May 2019, London, Ontario, Canada.
- Pediatrician, Own Clinic, Jul 2014 - Sep 2017, Aleppo, Syria.
- Resident Doctor in Pediatric Department, Aleppo University Hospital, Oct 2010 - Apr 2014, Aleppo, Syria.